SYNTHESIS AND CHARACTERIZATION OF PYRIDINIUM DERIVATIVES FOR APPLICATION IN NON-AQUEOUS REDOX FLOW BATTERIES

by

S. Isaac Michael Blythe, B.S.

A thesis submitted to the Graduate Council of
Texas State University in partial fulfillment
of the requirements for the degree of
Master of Science
with a Major in Chemistry
August 2018

Committee Members:

Todd W. Hudnall, Chair

Benjamin Martin

Christopher Rhodes

Shane Yost

FAIR USE AND AUTHOR'S PERMISSION STATEMENT

Fair Use

Duplication Permission

DEDICATION

For Celina: my first best friend; the Romy to my Michele; the Jane to my Daria. I miss you.

ACKNOWLEDGEMENTS

No lab experience is the same and I feel eternally grateful to the powers that be that I have had the opportunity to work in the Hudnall research group – the group has made graduate school breeze by and has been invaluable in my personal and academic endeavors. Especially, I would like to acknowledge one of my best friends both in and out of lab, Brenton Gildner, for his friendship, knowledge, and his endless nonsensical talents. I would also be remiss if I neglected to thank Dr. Tharushi Perera who refuses to acknowledge that she is, in fact, one of my chemistry heroes. I most certainly wouldn't be completing this program without the most important component of the Hudnall research lab – the man, the myth, the legend – Dr. Todd Hudnall. Dr. Hudnall has been the best influence in my academic career. Thank you for all the intriguing conversations and debates, and, above all, thank you for your persistence and your faith in me when I didn't have faith in myself. You have been absolutely critical in my development as a scientist, a student, and a human 'bene'.

I'd like to thank my family for understanding, if not supporting, my M.I.A. status during most of the last two years. I'd like to also thank my roommates, Zoe, Harold, Skyler, and Kat, for being my second family and making sure I remember to eat.

Speaking of eating, I would like to thank the NSF CAREER CHE-1552359 grant, the Wilcox Family Endowment, the Department of Chemistry and Biochemistry, and The Graduate College Scholarship of Texas State University for their funding of my graduate education and research.

TABLE OF CONTENTS

Page

LIST OF TABLES

Table **Page**

LIST OF FIGURES

Figure **Page**

LIST OF ABBREVIATIONS

Abbreviation	Description
ESS	Energy storage system
RFB	Redox flow battery
NASA	National Aeronautics and Space Administration
OCV	Open circuit voltage
ECW	Electrochemical window
NHC	N-heterocyclic carbene
CAAC	Cyclic alkyl amino carbene
MAAC	Mono-amido amino carbene
DAC	Di-amido carbene
HOMO	Highest occupied molecular orbital
LUMO	Lowest unoccupied molecular orbital
DFT	Density functional theory
USD	United States dollar
DCM	Dichloromethane

ABSTRACT

As renewable energy sources are further explored for integration into the electric grid on which we all rely, the question of how to meet energy storage demand in an equally "green" way arises. One potential solution to this demand is redox flow batteries. Redox flow batteries stand to become scalable grid-level energy storage systems due, in large part, to the separation of power and energy in the system inherent in structure. Many types of redox flow batteries have been thoroughly studied, with the bulk of them being aqueous systems relying on inorganic compounds. A major shift in the design of these batteries is the transition from inorganic and aqueous based systems to all-organic non-aqueous batteries to take advantage of the extended electrochemical window of solvents such as acetonitrile.

The objective of this thesis is to explore the electrochemical properties of di-pyridinium carbonyl species to examine their potential as redox flow battery anolytes. A suite of dipyridinium carbonyl compounds were synthesized and characterized electrochemically. Based on the literature surrounding pyridinium based anolytes, it was hypothesized that bis-4-(N-methyl pyridinium) carbonyl would prove to be the compound with the greatest competency regarding stability of the radical cation species and reversibility of the redox events in solution. This was found not to be the case; bis-2-(N-methyl pyridinium) carbonyl proves to be significantly more competent in terms of stability and reversibility. To further investigate this, a series of ortho- and para-benzoyl functionalized N-methyl pyridinium compounds were studied computationally using the hybrid (U)B3LYP functional and the 6-311++g(*) basis set. Hammett analysis of these various compounds showed that the stability of radical species does

improve with increasing electron withdrawing character of the substituent but is improved in the ortho- functionalized over the para- functionalized. These computational findings in conjunction with the experimental observations of stability and reversibility of di-pyridinium carbonyl electrochemical events indicates that the presence of a highly electron withdrawing moiety stabilizes the carbon ortho to the heteroatom as a point of radical localization. These observations may be used in future work to design ortho-functionalized derivatives with improved electrochemical properties in regard to redox flow battery applications.

I. INTRODUCTION TO ELECTROCHEMICAL REDOX FLOW BATTERIES AND ELECTROCHEMICALLY ACTIVE ORGANIC SPECIES

Introduction

Before his passing in 2005, Nobel Laureate Prof. Richard Smalley would challenge members of his seminar audiences to determine the most pressing issues for humanity to solve in the coming century.[1] Almost every audience agreed on a list of ten issues ranging from poverty to democracy; Prof. Smalley would show then that the number one issue among these was, and remains, the issue of energy. Without a reasonable, clean, and sustainable method of storing and distributing energy to meet the growing global need, other issues become increasingly more out-of-hand with regards to their negative impact on the world-wide quality of life.

As global energy demands increase and traditional energy sources such as coal deplete around the world, it is necessary that we begin to push for the practical integration of renewable energy into our electrical grid; however, renewable energy sources such as solar and wind typically have wide variance in their supply at any given moment. Energy storage systems (ESSs) are the solution to this issue, and various mechanisms of storage have been proposed. A scalable device then necessitates access to cheap, durable, and safe materials. One such device is the redox flow battery.

Defined redox flow battery systems

In redox flow batteries (RFBs) the energy and power are separated by storing the catholyte and anolyte solutions in reservoirs separate from the cell stacks.[2,3] In the actual stack itself, a porous membrane is employed to allow chemical charge balance throughout the charge and discharge processes.[4,5] In addition, this separation allows for intrinsic cooling of the battery system as fresh electrolytes are circulated into and out of the system.[2–4]

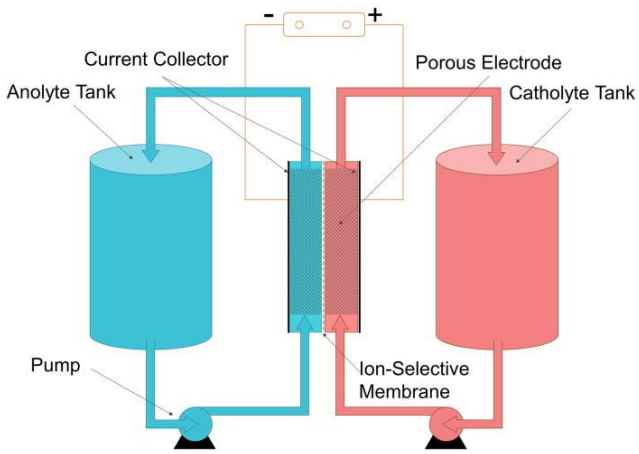

Figure 1. General schematic of a redox flow battery.[6]

RFBs have been studied since the late 1970s, when NASA developed what is largely considered the first of these devices.[7] The device was an iron(II/III)/chromium(III/II) couple with hydrochloric acid serving as the supporting electrolyte. Due to cross-over between the electrolytes, the open circuit voltage (OCV) being relatively low (0.9 to 1.2 V,) and the relatively slow kinetics of the chromium redox event compared to the iron redox event, this system was largely moved away from as newer and more efficient systems were developed.[3] Another concern in this system is the employment of a concentrated strong acid in the battery – the paradoxical use of an environmentally harsh chemical in a device meant to suffuse green energy into the market can hardly be overlooked.

A variation on the theme of inorganic RFBs was developed in the early 1980s, a bromine/polysulfide system, and has been modified over the last few decades.[8] The largest

issue to date with this system echoes concerns of the original NASA system – it very commonly suffers from cross-over and contamination through the membrane. In this case, the byproducts of contamination include H_2S and Br_2, which again call to mind safety concerns regarding this system.[3]

Perhaps the most commonly studied and readily available RFBs are those that are entirely vanadium-based.[9–15] By having the element of reduction/oxidation be the same in both the anolyte and catholyte of the battery system, the issue of cross-over is mitigated if not entirely circumvented. These systems are based on the V(IV/V) and VO^{2+}/VO_2^+ couplings with sulfuric acid as a supporting electrolyte. Highly soluble, up to 4 molar in sulfuric acid, these systems are arguably the most promising of aqueous RFBs studied to date; however, they – like all systems – come with their own set of disadvantages. An example of this is the limitations of electrode materials. The highly corrosive nature of the system severely depletes the options for electrodes, as they must be capable of withstanding the harsh conditions of the cell. More pressingly from the economic side of things are the high cost of materials necessary for the vanadium flow battery to function. Nonetheless, several companies are pushing for the design and implementation of large scale RFBs to better demonstrate to the public the benefits of these renewable energy systems. In the summer of 2017, for example, German based Ewe Gasspeicher GmbH announced plans to develop and implement an underground RFB, a project titled "brine4power," capable of powering 75,000 homes for a day.[16] The battery would be based on the vanadium system but utilize more recent advances that show the potential of using brine as a supporting electrolyte. This battery, when completed, is slated to be the largest battery in the world.

Broadly, aqueous RFBs are the community's largest focus, which comes with its advantages. With the emphasis having largely been on these systems since the 1970s, the

breadth of literature available makes the development and implementation of iterative design methods more accessible in industrial and academic settings. It would also be misguided to fail to acknowledge that aqueous RFBs have the advantage of utilizing an abundant and cheap solvent in their development versus the more expensive solvents employed in non-aqueous systems. However, it would be equally misguided not to acknowledge the limitations the community has placed on itself by focusing so heavily on aqueous systems for so long. The relatively small electrochemical window (ECW) of water (1.23 V) limits the types of chemistries that can be studied and implemented in RFBs when compared to the ECW of solvents such as acetonitrile (6.1 V).[17] Further, with the focus of RFBs being stated as the production of a grid-scalable method for green energy storage, it is counter-intuitive to develop systems that rely so heavily on metals which grow more and more rare and strong acids and oxidizers which are harmful to the environment.[18–20] Predominately in an effort to study expanded multi-electron systems without the limitation of water's ECW, there has been a noticeable push over the last decade to develop cheap and efficient non-aqueous RFBs.

Development of non-aqueous systems

The focus of non-aqueous RFB materials has incorporated elements of the aqueous analogue systems.[17,21–27] Many systems, for example, employ vanadium, multi-oxidation state capable metals such as chromium, or late transition metal, such as rhodium, based electrolytic solutions in organic solvents such as methane sulfonic acid or, more commonly, acetonitrile.[27] This direction has proved valuable as increasing studies show the cyclability of these designs and increased redox activity outside of the formerly limited ECW. In addition, many studies have been made employing all-organic materials for catholytes. Many of these systems are nitrogen, sulfur, or oxygen containing heterocycles and aromatic derivatives, such as quinone, alkoxyarene, and thiophene derivatives.[27]

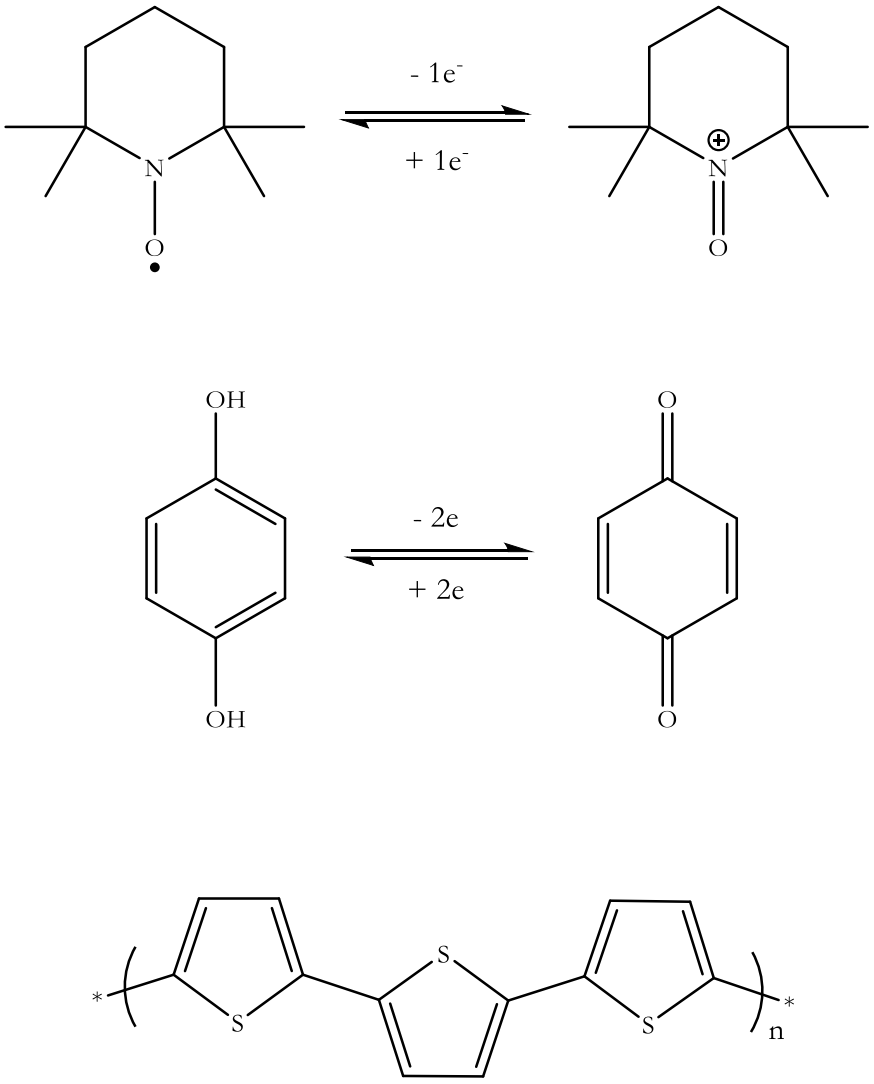

Figure 2. Some examples of redox active catholyte materials.

It cannot be stressed enough what a large advantage the expansion of chemical opportunity the enlarged ECW offers. By employing organic solvents in RFBs we can not only begin exploiting new molecules that may not be appropriate in aqueous environments, but we can also expand the possible redox chemistry of traditional RFB systems by virtue of the larger ECW.[28,29] This is to say little of the economic advantage of using relatively cheap materials in development of new technologies over the rather costly inorganic aqueous

analogues. More fundamentally, however, it cannot be ignored that the stability of organic radicals in both solid and solution states has been known since 1900.[30] We, as chemists, would then be remiss to not take advantage of this known stability in our design and implementation of a technology that relies heavily on the stability of radical species in solution.

The biggest gap in the current literature, thus arguably the largest disadvantage, regarding organic non-aqueous RFBs is that of possible anolyte materials. Current efforts to synthesize, understand, and employ such materials are underway in research groups around the world. Some of the most promising work on this front in the last five years has come from the group of Prof. Melanie Sanford at the University of Michigan, whose work designing multiple generations of suitable pyridinium derived anolytes was seminal in the work delineated in this thesis.

Pyridinium derivatives – redox-active species

Perhaps the most salient pyridinium derivatives to mention in context of anolyte development are those belonging the viologen family. Paraquat is likely the most well-known viologen derivative due to its use as an herbicide and is the dimethylated derivative.

Paraquat has a well-established electrochemical profile, having been studied as a redox active species since the 1930s.[31,32] Viologen derivatives are known to undergo a reversible 1 electron reduction event to a free radical species in which the radical resonates into the ring to form a carbon centered radical on an isolated diene ring, as shown in ***Figure 3***.

The second reduction of these compounds was initially theorized to lead to the formation of a diradical, but magnetic susceptibility studies show that the second reduction leads to a quinone type structure between the two heterocyclic moieties.

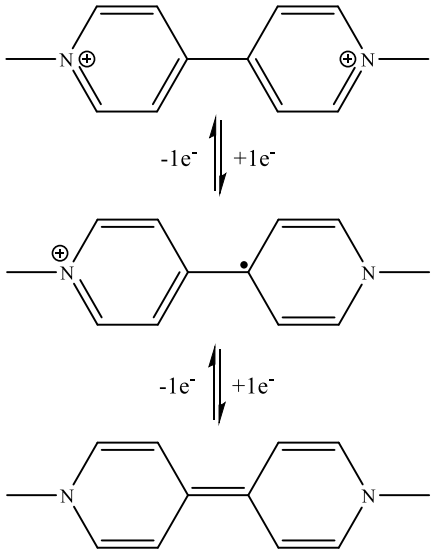

Figure 3. Redox events of paraquat.

To date, however, much of the study and implementation of viologen derivatives in the context of potential redox-flow batteries has been in polymeric derivatives, limited non-aqueous systems, or more broadly in aqueous systems.[28,29,41,42,33–40] Nevertheless, the excellent promise of a cyclable anolyte material has led many scientists to investigate other pyridinium derivatives. As previously mentioned, some of the most elegant examples of this work have been accomplished by the group of Prof. Melanie Sanford.[23,43–46] Through iterative modification and design, several organic molecules were prepared starting with a functionalized bipyridine and eventually identifying the *p*-acyl pyridnium cation to be an anolyte stable in mixed redox states for several hours in solution.[23]

These findings led to further studies in the Sanford group, concurrent to the work of this

thesis, that had significant commentary regarding the steric and electronic effects assisting in

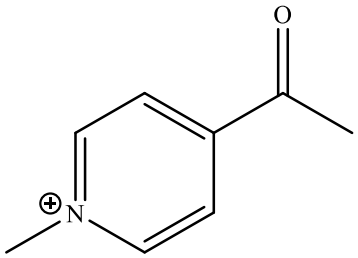

Figure 4. Compound determined by Sevov et. al to have best promise as material for redox flow battery in 2015 work.

stabilizing these species as redox active materials, which will be discussed in further detail in later chapters. Broadly, the work published by Sanford served as the first major component for the intellectual inspiration of this thesis. The second, seeming at first to be unrelated work, was accomplished by the group of Prof. Guy Bertrand at the University of California – San Diego, which will be discussed shortly.

Carbenes – tunable redox stabilizing platforms

In the late 1980s, Baceiredo and coworkers synthesized what can be argued to be the first isolable carbene species.[47] The carbene, shown in ***Figure 5***, is stabilized by the push-pull effects that the hetero atoms in the molecule exert on the carbene carbon.

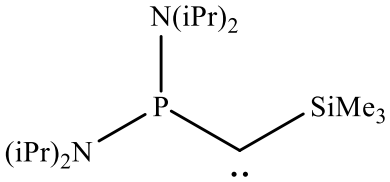

Figure 5. First stable singlet carbene isolated by Baceiredo et. al.

This set the groundwork for the later unambiguous synthesis and isolation of a stable carbene by Arduengo *et al.*, who took advantage of the push-pull capabilities of nitrogen as an atom with high electronegativity and a lone-pair for electron density donation.[48] Ardugeno's work

was truly the point at which carbene chemistry was able to evolve into the field of today, as it provided a template for future chemists to design and synthesize carbenes with novel reactivity and tunable electronic properties.

Depending on the backbone of the carbene, the frontier orbital energies can be modified.[49–58] The most commonly used carbenes employed in catalyst development, N-heterocyclic carbenes (NHCs), are typically more nucleophilic with higher energy LUMO levels. More electrophilic carbenes, such as diamidocarbenes (DACs), have smaller HOMO-LUMO gaps and are more capable of pi-backbonding by virtue of their lower energy LUMO levels.

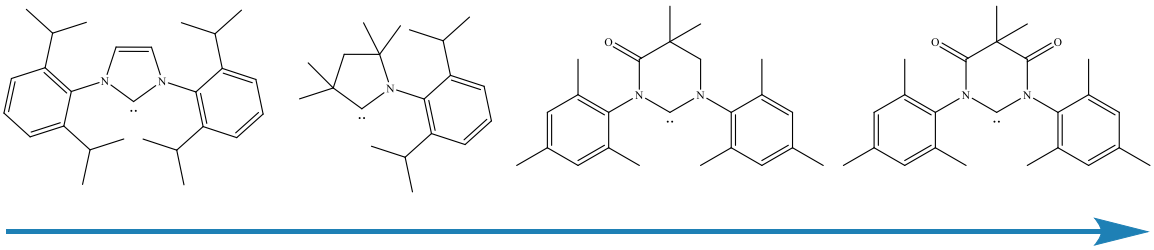

Figure 6. Increasing electrophilicity, from left to right, of some carbenes. General carbenes, left to right: N-Heterocyclic Carbene (NHC), Cyclic Alkyl Amino Carbene (CAAC), Mono-Amido Amino Carbene (MAAC), Di-Amido Carbene (DAC).

Our group has previously shown that the electrophilic or nucleophilic nature of the carbene moiety has a noted impact on the potential of reduction in electrochemically active compounds.[59] The NHC shown above, MAAC, and DAC were each acylated at the position of the carbene carbon to form a cationic species, a formamidinium, and studied by cyclic voltammetry. By varying the electrophilic nature of the carbene moiety, the first reduction event's potential can be tuned by nearly a volt – the DAC derivative shows an initial reduction potential of -0.48 V, and the NHC derivative shows an initial reduction potential of -1.32 V. The nature of the carbene moiety also seems to control the reversibility of the second redox

event to form the anionic species, as DAC will partially allow a reversible second event and NHC will not form the anion reversibly at all.

We are hardly the only group interested in the use of carbenes as redox stabilizing and tuning platforms. Many groups have shown that carbene derived radical species are highly stable. The most relevant of these to this thesis are the radical species incorporating a cyclic(alkyl)amino carbene (CAAC) which have been published by Mahoney *et. al.* Mahoney designed a number of acyl functionalized CAAC derivatives to study their ability to stabilize a radical species.[60] In the 2015 work, density functional theory (DFT) was employed to determine which acyl functionalization of CAAC would allow for a radical with the highest spin density on the carbonyl carbon. In addition, theoretical reactions with triplet oxygen were calculated using DFT and the enthalpy of reaction compared to the Hammett parameter of the substituent, shown in ***Figure 7A***. According to the calculations, groups with highly electron withdrawing character were the most favorable candidates for stable radical formation based on their higher enthalpy of reaction with triplet oxygen. Following this data, the compounds in ***Figure 7B*** were synthesized and their stability in water and in air studied. Notably, incorporation of a second cationic CAAC derivative was shown to have phenomenal stability in both air and water – the radical is not only isolable but is worked up under aqueous conditions and can be left under atmosphere for almost two years without any significant decomposition.

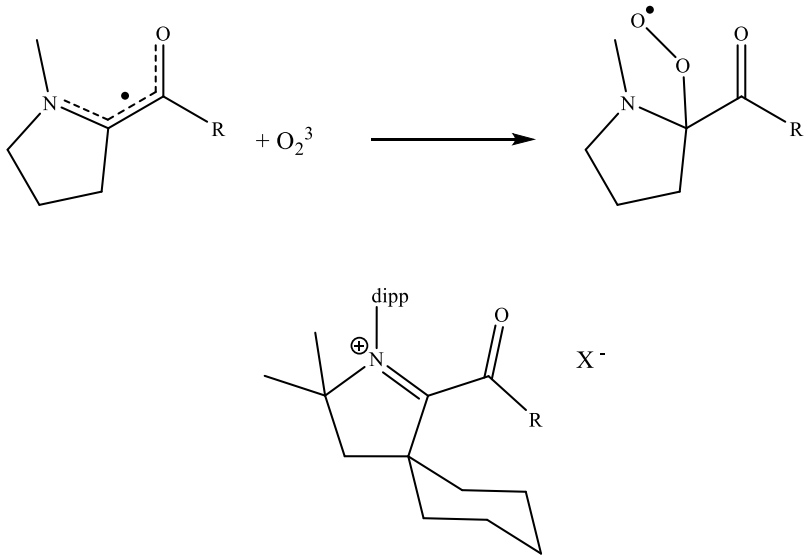

Figure 7. A) Generic reaction with triplet oxygen studied by Mahoney et. al [R = NO_2, CN, $COCH_3$, C_3F_7, CHO, C_6F_5, 4-NO_2(C_6H_4), CCH, CHCHCHO, H, Ph, Me, c-Pr, OMe, NH_2, NMe_2] and B) general structure of cations synthesized by Mahoney et. al. [dipp = diisopropylphenyl. R = Ph, X = Cl; R = 3,5-$(CF_3)_2$-(C_6H_3), X = Cl; R = C_6F_5, X = BPh_4; R = C_3F_7, X = Cl; R = CAAC, X = BF_4.] Note: when R = CAAC, ketone tautomerizes to enol.

Objectives

As previously stated, the work of Sanford and the work of Bertrand is largely inspirational to the content of this thesis. This is because, through extreme resonance structures, the pyridinium compounds synthesized by Sanford can be treated and understood as remote NHCs datively bonding into the Lewis acidic acyl cation moiety as shown in ***Figure 8***. By treating these derivatives as carbene-like, we then extrapolate that the findings of Bertrand are applicable to these systems. Namely, with increasing electron withdrawing character of the acyl substituent, we expect to see increasing stability of the radical species and thusly improved stability relative to the compounds studied by Sanford. Additionally, with the incorporation of a second cationic moiety, we should expect to see an increase in the number of electrons that can be added into or removed from the molecule by up to 2 e^-.

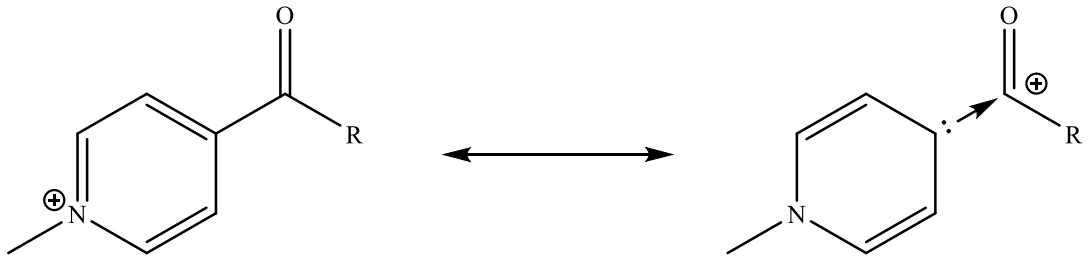

Figure 8. Resonance structure showing the treatment of acyl functionalized pyridinium as a remote NHC.

Based on the treatment of pyridinium as a remote-NHC, we have here synthesized the 6 isomers of dipyridyl ketones and alkylated in an attempt to synthesize di-pyridinium carbonyls to best take advantage of the known excellent redox properties of the pyridinium moiety while imparting the expected stability from the second cationic center. Mono-pyridyl ketone radical systems have been derived to theoretically examine the effects of electron withdrawing versus electron donating substituents on the acyl moiety with regards to stability and electronic properties of the pyridyl ketone radical compound.

II. DI-PYRIDINIUM CARBONYL SYSTEMS: SYNTHESIS, CHARACTERIZATION, AND ELECTROCHEMICAL PROPERTIES

Introduction

Dipyridyl ketones have been observed with certainty dating back to the late 1940s when Linkser and Evans synthesized di-3-pyridyl methanone by distilling nicotinic acid through thorium dioxide at high temperatures.[61] Rather quickly, this method was discarded as the preferred method of synthesis due to its low yield and high cost in favor of methods of synthesis involving the coupling of lithiopyridines with cyanopyridines developed independently by Wibaut *et. al* and Henze *et. al* in the at 1940s and early 1950s.[62,63] These methods remain the most common synthetic routes, which may also serve as commentary on the rather small span of literature surrounding these molecules. There are six isomers, shown in ***Figure 9***, each of which has various synthetic challenges and uses in research and industry which will be discussed briefly here.

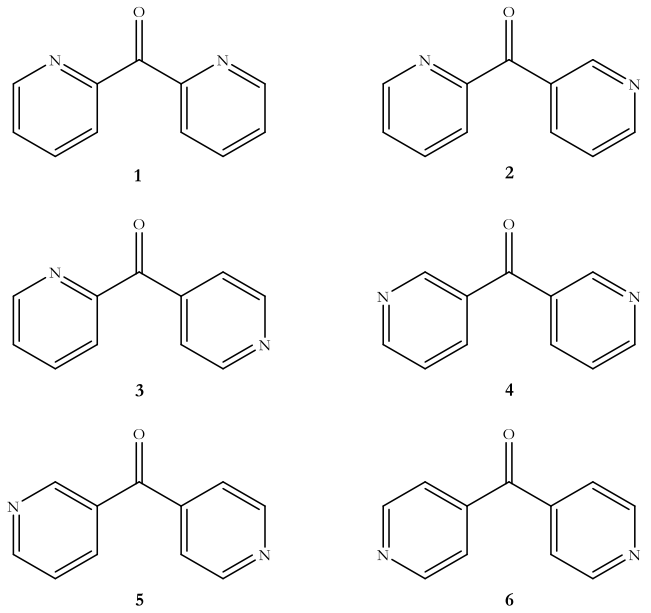

Figure 9. 6 isomeric forms of dipyridyl ketone.

All 6 isomers of dipyridyl ketone were synthesized in varying yield by Wibaut, but many

were not studied beyond synthesis for nearly two decades. **1** was predominately studied in the early 1970s by Summers *et. al* for their potential herbicidal properties.[64] The stability of diaryl ketone radical anions was well defined by this point, and Summers speculated that the di-pyridinium carbonyls, N-alkylated analogues of dipyridyl ketones, may be stable in the radical cation form; however, the species were simply reduced using zinc without much discussion regarding the electrochemical properties of reduction of any analogues synthesized.

Unlike **1**, **2** does not have a studied dicationic analogue. The neutral ketone has also not been heavily employed in any form of redox related study; however it has been used to assist in the assembly of helical structures as a coordinating ligand.[65]

3 has been studied more in depth by polymer chemists and by photophysicists than by electrochemists. The dicationic species is not reported, but the neutral ketone has been studied in the development of silver coordinating polymers and as a potential photosensitizer.[66–68]

Both **4** and **5** have been synthesized, but the neutral ketones seem to be rarely studied in the literature, likely to the very low yield reported in various synthetic methods.[62,63]

The most relevant and promising of these in terms of redox flow batteries is $\mathbf{6}^{2+}$, which has been reported before by Filipescu *et. al* in the late 1960s and early 1970s, when the properties of the singly reduced species were studied to uncover any sort of analogous properties with respect to the literature surrounding the physiological impact of other radical cations such as paraquat.[69–71] In keeping with the times, the compounds were simply reduced using zinc and not studied electrochemically.

Concurrent to and independent of the development of this work, Araujo and coworkers published a rather expansive article combining theoretical and experimental data of over 137 compounds, including **1-6**, for application in redox flow batteries.[72] Specifically, they studied the redox activity of these and other molecules for potential incorporation into a conducting

polymer for a high capacity battery. They found that the dipyridyl ketones as neutral species have reduction potentials nearing -2.0 V, which may be desirable for certain applications.

As such, the dialkylated species shown in ***Figure 10*** still hold promise for exploration and exploitation of their redox activity. Based on the reduction and stability of mono-pyridinium ketones which were specifically para-substituted, we expected that of these $\mathbf{6}^{2+}$ would be the dication that gave us the most stable radical species and highest degree of reversibility in both the one and two electron processes.

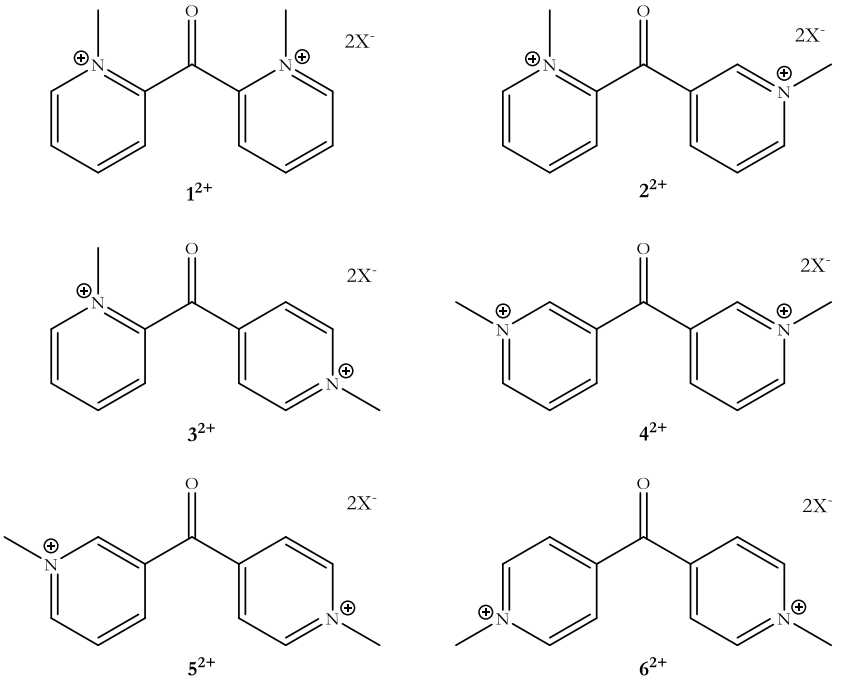

Figure 10. Isomers of di-pyridinium carbonyls. X = OTf or BF_4^-.

Asymmetric di-pyridinium carbonyl systems

One of the key aspects of redox flow battery design is accessibility of materials. The di-pyridinium carbonyl species proved to be more synthetically challenging than originally anticipated. It was expected that the meta-substituted pyridinium compounds would be the least likely to participate in reversible redox activity based on the inability of these radical

structures to resonate into the carbonyl of the system, shown in ***Figure 11***, leading to increased coupling in the radical containing compounds.

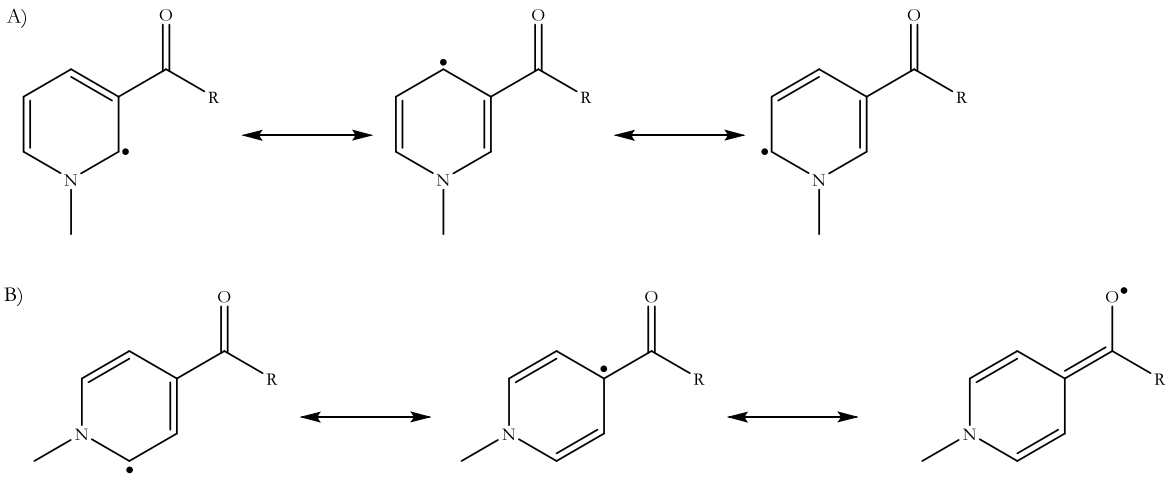

Figure 11. **A**) Resonance of radical on meta-acylated pyridinium derivative; **B**) Resonance of radical on para-acylated pyridinium derivative

Despite evidence that the inclusion of a *meta*-pyridyl substituent may negatively impact the electrochemical properties of the compound[23], we decided to study the incorporation of these substituents to see if stability imparted by the *ortho*-pyridyl, or later *para*-pyridyl, could allow for a reasonably useful system. **2** was synthesized by reaction of 2-lithiopyridine and methyl nicotinate in 49.7% yield (275 mg). The resulting tan needles were alkylated using 0.41 mL of methyl triflate in a dry glovebox, and 760 mg (99.4% yield) of the dialkylated salts were recovered by filtration. A solution of the dialkylated salt was then studied in an inert atmosphere by cyclic voltammetry.

It becomes rapidly apparent at a 100 mV/s scan rate that $\mathbf{2}^{2+}$ is a poor candidate for redox flow batteries. ***Figure 12*** shows that under standard cyclic voltammetry conditions $\mathbf{2}^{2+}$ undergoes a single irreversible reduction before it decomposes into a highly oxidizable compound, or several highly oxidizable compounds.

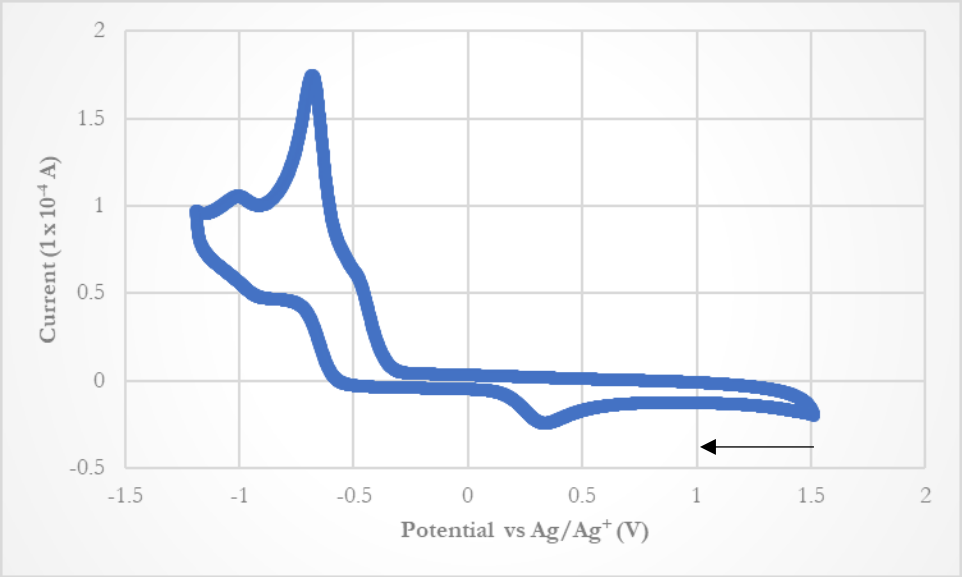

Figure 12. Cyclic voltammogram of $\mathbf{2}^{2+}$. 0.01 M in MeCN; 0.100 M $LiBF_4$; 100 mV/s; 2nd scan. Arrow indicates sweep direction.

To affirm that the compound decomposes after a single electron reduction, 54 mg of $\mathbf{2}^{2+}$ in acetonitrile were reduced with zinc metal in an inert atmosphere. Upon addition of zinc to the translucent tan solution in the reaction flask, the reaction takes on a bright yellow coloration before rapidly turning bright orange. When concentrated *in vacuo*, the resultant product mixture is a bright yellow gummy solid which is soluble in acetonitrile. An EPR sample was prepared in a capillary tube of acetonitrile suspended in THF; however, the EPR collection showed no signals indicating that a radical had not been formed. To further corroborate this, ^{1}H NMR was collected in deuterated acetonitrile. The spectrum, ***Figure 13***, shows several peaks; analysis of the region characteristic of nitrogen bound methyl groups, approximately 4.0-4.5 ppm, indicates that at least 6 unique methyl groups now exist in the resultant product mixture. The following shifts (δ ppm, CD_3CN) are all singlets that seem to correspond to methyl groups on the same compound based on calibration from aromatic protons: 4.27 and 4.42; 4.31 and 4.40; 4.33 and 4.37. Two peaks also develop in the region between 5.5-7.0 ppm, indicating the alteration of bonds from the aromatic structure of $\mathbf{2}^{2+}$ to

a structure more congruent with non-aromatic olefins.

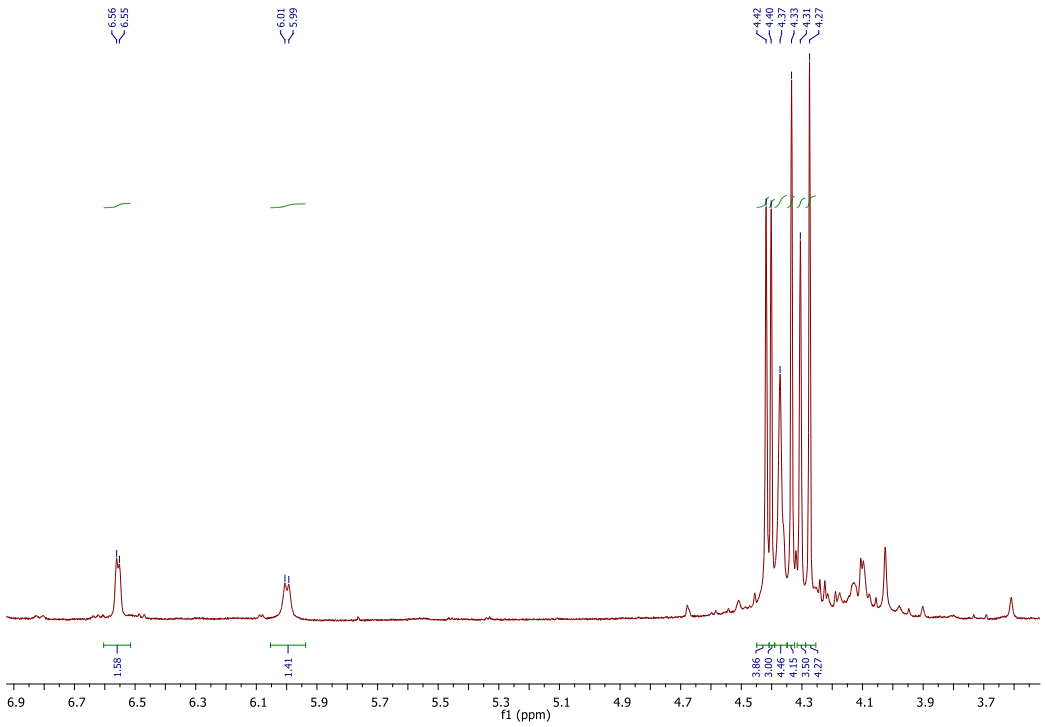

Figure 13. ^{1}H NMR in CD_3CN of Zn reduced $\mathbf{2}^{2+}$.

The mixture does continue to undergo chemical changes if exposed to air or even if allowed to sit undisturbed in an inert atmosphere over the course of several weeks – the mixture changes from an orange gummy solid to a brittle brown solid that is insoluble in acetonitrile, THF, or chloroform. Based on these data, $\mathbf{2}^{2+}$ is not a suitable material for redox flow batteries, and so further characterization of the resultant products was not completed.

Based on the excellent redox activity of *para* substituted pyridyl derivatives shown by Sevov and coworkers and moderate redox activity of *ortho* substituted pyridyl derivatives shown in the same work, the combination of these two moieties in conjunction with the conversion of both pyridyl substituents to pyridinium substituents held promise as a potential redox system of interest. **3** was synthesized by reaction of 2-lithiopyridine with 4-

cyanopyridine and subsequent hydrolysis to yield 414.6 mg (32.1%) of a tan powder. **3** was treated with 2.5 equivalents of methyl triflate in DCM below room temperature in an attempt to isolate the dication, but only the monocation was recovered from solution. **3** was treated with 1.75 equivalents of trimethyloxonium tetrafluoroborate in DCM at room temperature to facilitate easier recovery and isolation of the dication; however, the dication does not form through this method. Only the monocation, $\mathbf{3}^{+}$ can be isolated from this reaction. Due to the expensive materials in these methods of methylation and the desire to keep costs of redox flow battery materials low, $\mathbf{3}^{2+}$ was not further pursued.

The remaining asymmetric di-pyridinium carbonyl, $\mathbf{5}^{2+}$ proved to be much more readily accessible synthetically and was pursued despite the previous results from $\mathbf{2}^{2+}$. **5** was synthesized in a similar fashion to **3**, using 3-lithiopyridine as the lithium precursor, and was isolated as an off-white powder in 22.2% yield. $\mathbf{5}^{2+}$, a white powder (224.0 mg, 86.2% yield) was prepared via reaction with excess methyl triflate below room temperature for 15 hours and recovered by filtration. Using the same conditions as $\mathbf{2}^{2+}$, cyclic voltammetry data was collected showing a much more stable, though not reversible, electrochemical profile for $\mathbf{5}^{2+}$.

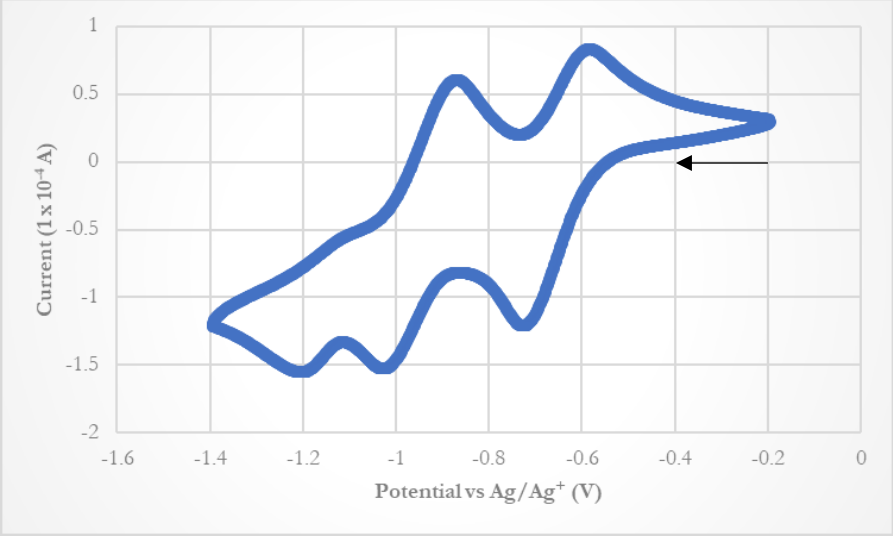

Figure 14. Cyclic voltammogram for $\mathbf{5}^{2+}$. 0.01 M in MeCN; 0.100 M $LiBF_4$; 100 mV/s; 2nd scan. Arrow indicates sweep direction.

The scan shown in ***Figure 14*** indicates that the first of the two redox events that were analyzed has very poor reversibility ($i_{p,a}/i_{p,c}$ = 0.5) and the second event is poorly reversible ($i_{p,a}/i_{p,c}$ = 1.1.) In addition to the poor reversibility of these events, the $E_{1/2}$ separation for the first and second events is rather small at 0.2890 V. With an even smaller event separation, there seems to be a third redox process occurring after the second reduction, which may contribute to the poor reversibility of events when cycling $\mathbf{5}^{2+}$. Despite the poor reversibility by calculating the ratio of peak currents, both events that were analyzed do roughly exhibit linearity when the current, *i*, of the cathodic peak at variable scan rates, ν, is plotted against $\nu^{1/2}$ (event 1: R^2 = 0.9797; event 2: R^2 = 0.9879) as shown in ***Figure 15***.

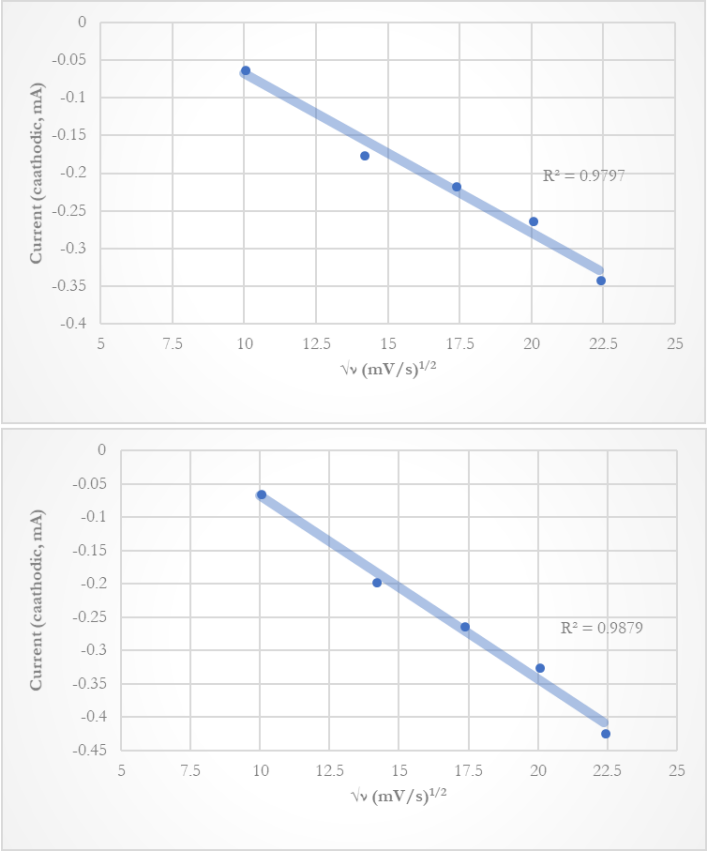

Figure 15. Randles-Sevcik linearity of $\mathbf{5}^{2+}$. Calculated using scan rates of 100 mV/s, 200 mV/s, 300 mV/s, 400 mV/s, and 500 mV/s.

This observed linearity is characteristic of reversible or at least quasi-reversible single electron processes which are diffusion controlled based on the Randles-Sevcik equation (eq 1). Eq. 1 relates the current observed, i_p (A), to the scan rate, ν (V/s), concentration, C (mol/cm^3), diffusion coefficient, D (cm^2/s), number of electrons involved in the process, n, area of electrode, A (cm^2), temperature of solution, T (K), Faraday's constant, F (C/mol), and the ideal gas constant, R (J/Kmol). Summarily, $\mathbf{5}^{2+}$ holds more promise than $\mathbf{2}^{2+}$ or **3** with regards to potential application in redox flow batteries based on its isolation and quasi-reversible redox activity.

$$i_p = 0.446nFAC\left(\frac{nF\upsilon D}{RT}\right)^{1/2} \quad (1)$$

Symmetric di-pyridinium carbonyl systems

The symmetric di-pyridinium carbonyl systems held much more promise from the early stages of conception in this project and it's plain to see why after the rather abysmal electrochemical properties of the asymmetric analogues. One symmetric analogue, however, proved to be even more problematic in terms of synthesis than the asymmetric analogues. The synthesis of **4** was attempted through several different routes with exceedingly poor yields, if any yield was obtained. Only one attempt to synthesize **4** was successful, via reaction of 3-lithiopyridine with methyl nicotinate over several hours, in enough yield to proceed to dialkylation; however, the dicationic species, through methylation with excess methyl triflate, was so hygroscopic that, even in drybox conditions of less than 5 ppm of moisture, water uptake prevented efforts to isolate and study the dication by CV with reproducible results. Since a defining factor of redox flow battery materials is a necessarily stable and easily accessible material, no further efforts to study $\mathbf{4}^{2+}$ were made in favor of focusing on the derivatives of **1** and **6**.

Compound **1** is undoubtedly the most accessible of the dipyridyl ketone analogues, as it is the only analogue commercially available at a price lower than 20 USD/g. Because of its commercial availability, the dicationic analogues of **1** were able to be studied more than the analogues that had to be synthesized. **[1^{2+}]2OTf^{-}** was the first of these to be synthesized through alkylation with methyl triflate to yield a grey-white powder in 84.8% yield. The dication was studied by cyclic voltammetry, ***Figure 16***, and had marked improvement over any of the asymmetrical analogues.

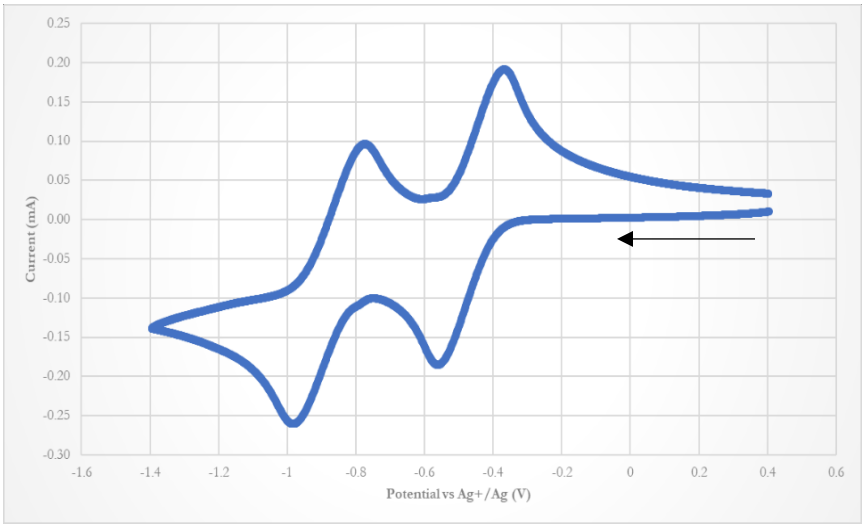

Figure 16. Cyclic voltammogram of **[1^{2+}]2OTf^{-}**. 0.01 M in MeCN); 0.100 M $LiBF_4$; 100 mV/s; 1st scan. Arrow indicates sweep direction.

The first and second redox events ($E_{1/2,\,1}$ = -0.4685 V; $E_{1/2,\,2}$ = -0.8835 V) both exhibit excellent reversibility by both Randles-Sevcik linearity as shown in ***Figure 17*** (R_1^2 = 0.9997; R_2^2 = 0.9999) and by their peak current ratios ($i_{p,a,1}/i_{p,c,1}$ = 0.97, $i_{p,a,2}/i_{p,c,2}$ = 0.95). Additionally, the events are fairly well separated, with 0.4150 V between them. This finding was initially surprising considering the findings of Sevov *et. al* which found that ortho-acylated pyridine derivatives did not exhibit good reversibility under CV conditions.[23] There are two major differences between the functionality studied by Sevov *et. al* and this work: one is that these derivatives have been alkylated as well as acylated; the second is that the substituent comprising

the acyl group is significantly different. The substituent initially studied by Sevov et. al was a methoxy group which can act as an electron donating group. That substituent may have contributed to the observed instability by donating electron density back into the carbonyl which makes it less likely to participate in radical stabilization. Seemingly congruent with the findings of Bertrand *et. al*, **[1^{2+}]2OTf**$^{-}$ stands out as a potential redox flow battery material.

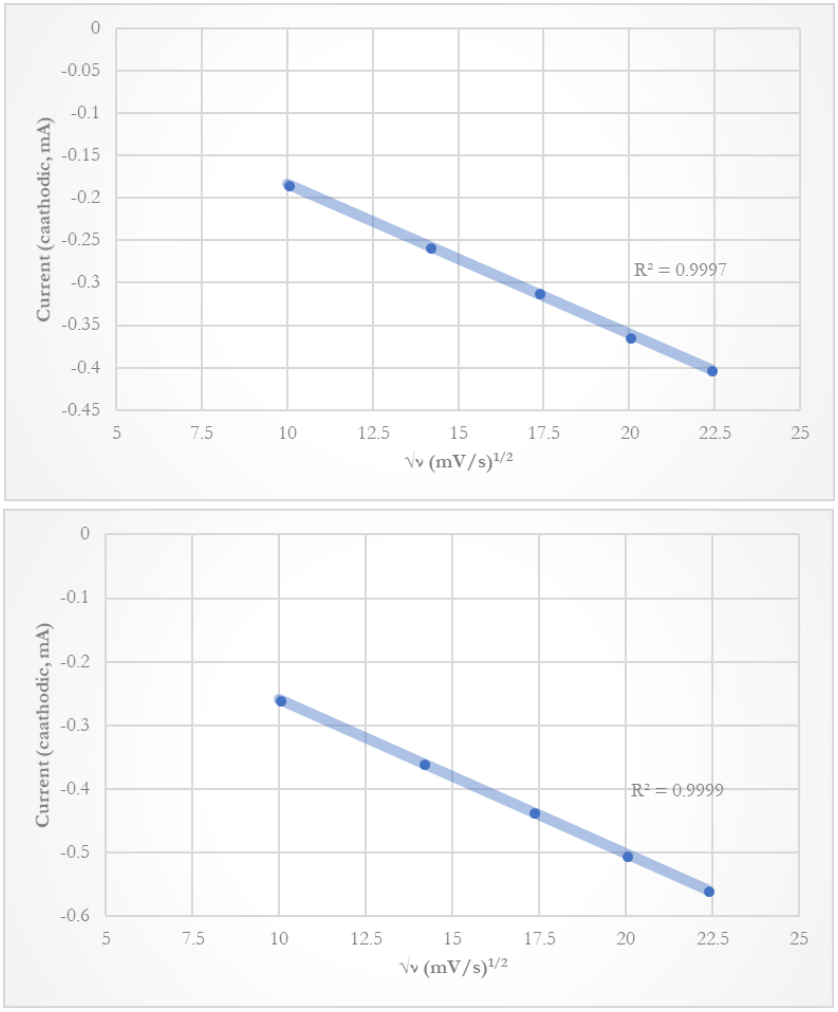

Figure 17. Randles-Sevcik linearity of **[1^{2+}]2OTf**. Calculated using scan rates of 100 mV/s, 200 mV/s, 300 mV/s, 400 mV/s, and 500 mV/s.

Since **1** is commercially available, a second dicationic derivative was made to study if counter anions had any effect on stability in solution of the compounds. **[1^{2+}]2BF$_4$ $^-$** was synthesized by reacting **1** with 2 equivalents of trimethyloxonium tetrafluoroborate in DCM at room temperature. An off-white powder was recovered by filtration in 87.8% yield and studied by CV.

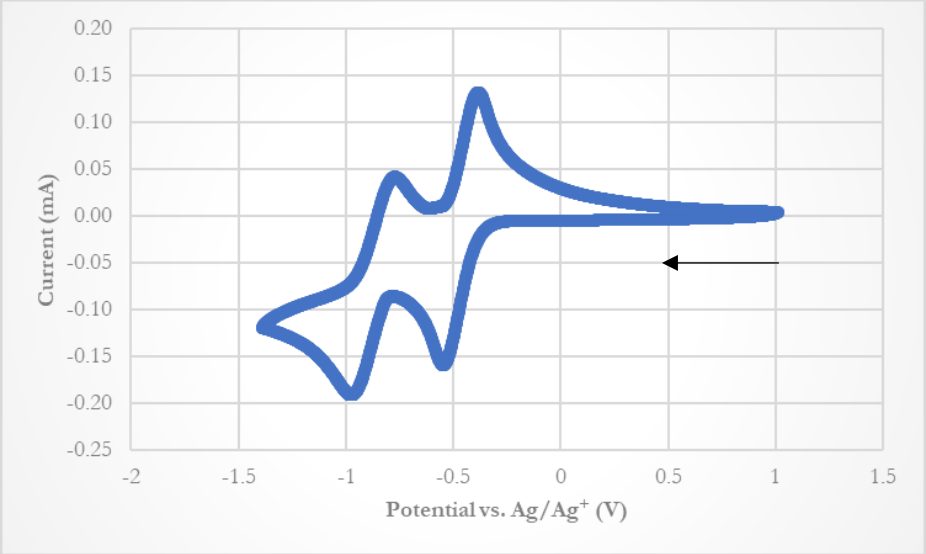

Figure 18. Cyclic voltammogram of **[1^{2+}]2BF$_4$ $^-$**. 0.01 M in MeCN; 0.100 M LiBF$_4$; 100 mV/s; 2nd scan. Arrow indicates sweep direction.

A change in the reversibility or the redox event potential by changing the counter anion was not expected, but both aspects of the CV changed noticeably which can be seen in ***Figure 18***. The reversibility of both events dropped when calculated by current peak ratios ($i_{p,a,1}/i_{p,c,1}$ = 0.94, $i_{p,a,2}/i_{p,c,2}$ = 0.86) and based on Randles-Sevcik linearity, shown in ***Figure 19*** (R_1^2 = 0.9987; R_2^2 = 0.9931). Both redox events were slightly anodically shifted with respect to **[1^{2+}]2OTf $^-$** ($E_{1/2,\,1}$ = -0.4773 V; $E_{1/2,\,2}$ = -0.8847 V,) and the event separation also slightly decreased to 0.4074 V. Due to the difference in reversibility, mostly in the reversibility of the second reduction, it seems that the **[1^{2+}]2OTf $^-$** out-performs the **[1^{2+}]2BF$_4$ $^-$** analogue.

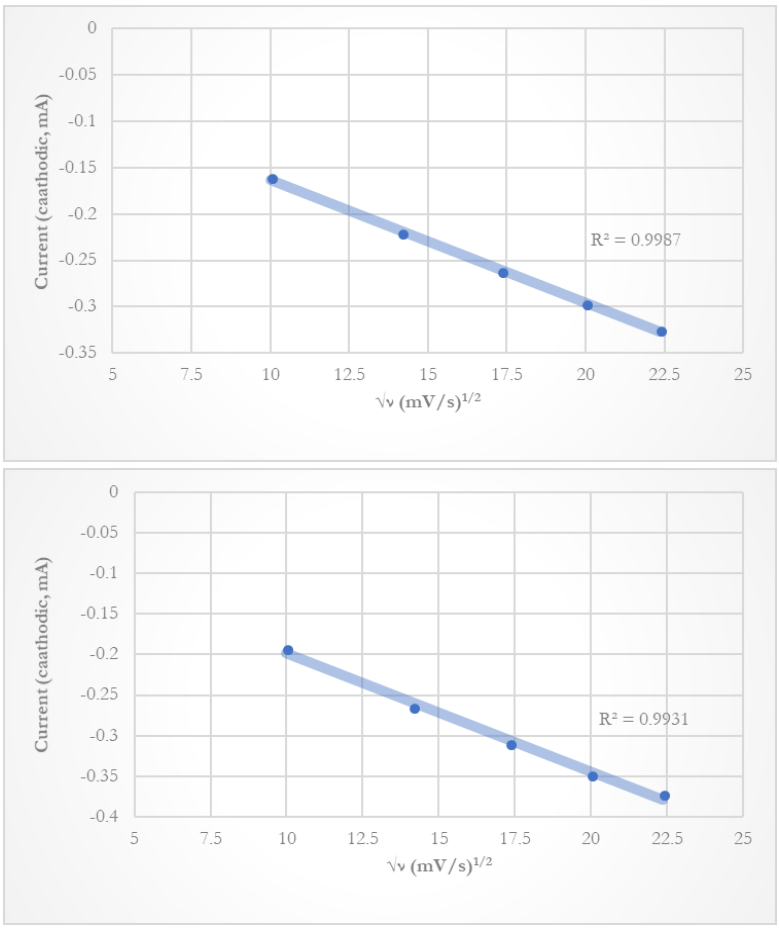

Figure 19. Randles-Sevcik linearity of **[1^{2+}]2BF$_4^-$**. Calculated using scan rates of 100 mV/s, 200 mV/s, 300 mV/s, 400 mV/s, and 500 mV/s.

It was not expected that synthesizing **6** would have a unique set of challenges regarding one of the starting materials. 4-bromopyridine is commercially available as a hydrochloride salt; this is because 4-bromopyridine will self-condense into a polymer upon prolonged exposure to light or temperatures above ca. 10˚C. Nearly every synthetic procedure for **6** that uses 4-bromopyridine neglects to mention this. This means that there are extra steps, and thus extra costs, associated with the reaction beyond those to synthesize any of the other analogues. **6** was synthesized by a modified procedure using 4-lithiopyridine and 4-cyanopyridine at low temperature and low light. A peach colored solid was recovered in low yield (13.2%) and

determined by ^{1}H NMR to be the desired product. **6** was then alkylated with excess methyl triflate to obtain $\mathbf{6}^{2+}$ in DCM below room temperature for 22 hours. The product was recovered by filtration in moderate yield (43.7%) and then studied by CV (***Figure 20***.)

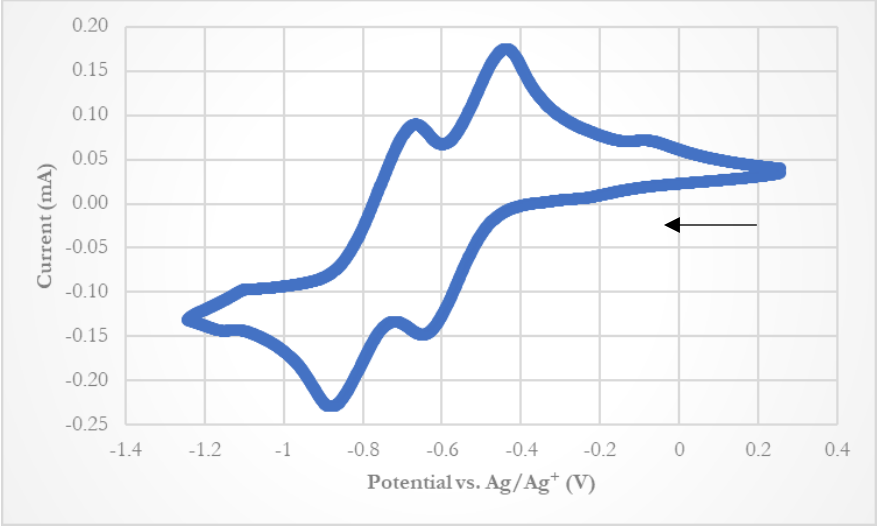

Figure 20. Cyclic voltammogram of $\mathbf{6}^{2+}$. 0.01 M in MeCN; 0.100 M $LiBF_4$; 100 mV/s; 2nd scan. Arrow indicates sweep direction.

The results of the CV for $\mathbf{6}^{2+}$ were quite unexpected. Despite the inferences made based on previous work, $\mathbf{6}^{2+}$ seems to be a considerably worse candidate for redox flow battery application than even the meta-substituted isomer $\mathbf{5}^{2+}$. In terms of reversibility as determined by current peak ratios, the first redox event is along the order of the second event of $\mathbf{5}^{2+}$($i_{p,a,1}/i_{p,c,1}$ = 1.15,) but is still quite far off the mark from the high reversibility exhibited by **[1^{2+}]2OTf^{-}**. The second redox event has the worst reversibility by current peak ratios of any compounds other than $\mathbf{2}^{2+}$ ($i_{p,a,2}/i_{p,c,2}$ = 0.38.) The Randles-Sevcik linearity, ***Figure 21***, is considerably higher than the current peak ratios may suggest for both events (R_1^2 = 0.9981; R_2^2 = 0.9989,) but it appears that the redox events of $\mathbf{6}^{2+}$ are not as reversible, and thusly not as desirable for this application, as those of **[1^{2+}]2OTf^{-}**. In addition to the poor reversibility of both redox events, the event separation is the lowest of the dications studied with a separation of just 0.2320 V.

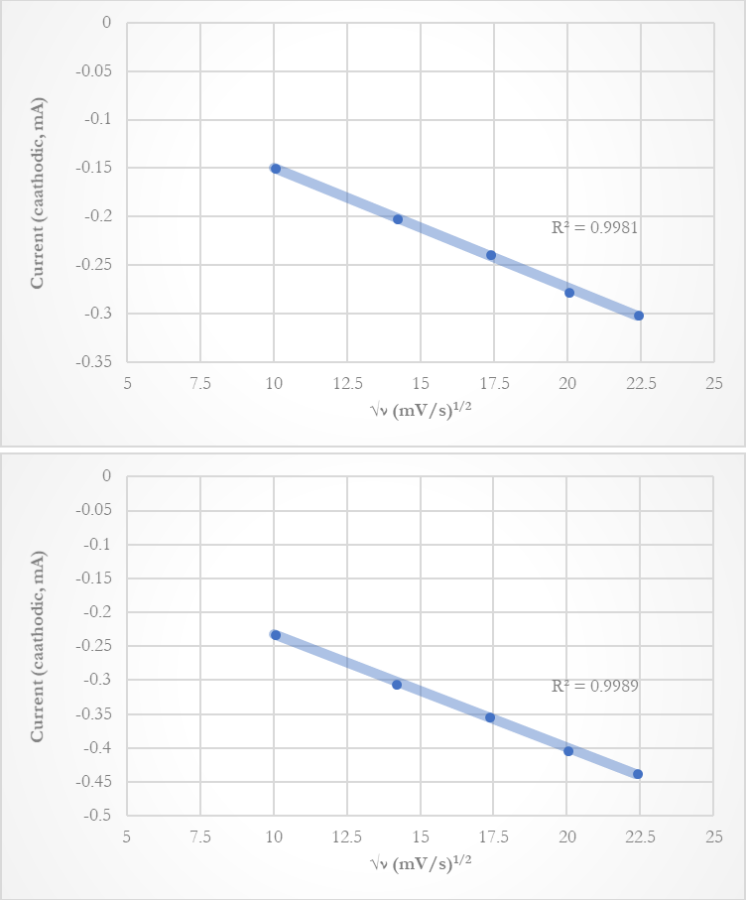

Figure 21. Randles-Sevcik linearity of $\mathbf{6}^{2+}$. Calculated using scan rates of 100 mV/s, 200 mV/s, 300 mV/s, 400 mV/s, and 500 mV/s.

Considering the high correlation of the Randles-Sevcik plots in ***Figure 21***, it is pertinent to address the differences in reversibility and cyclability. While the peak-current ratios and Randles-Sevcik linearity correlations are incongruous with one another, the cyclability of $\mathbf{6}^{2+}$ is shown in ***Figure 22***. There does not seem to be a significant change in the current produced from the redox events, which may indicate that the poor reversibility observed by peak-current ratios is due to saturation differences in the diffusion layer which alters the current output. This change may be further investigated by doing more diffusion-based studies in the future to probe if the redox events can be separated enough to alter reversibility by peak-current ratios.

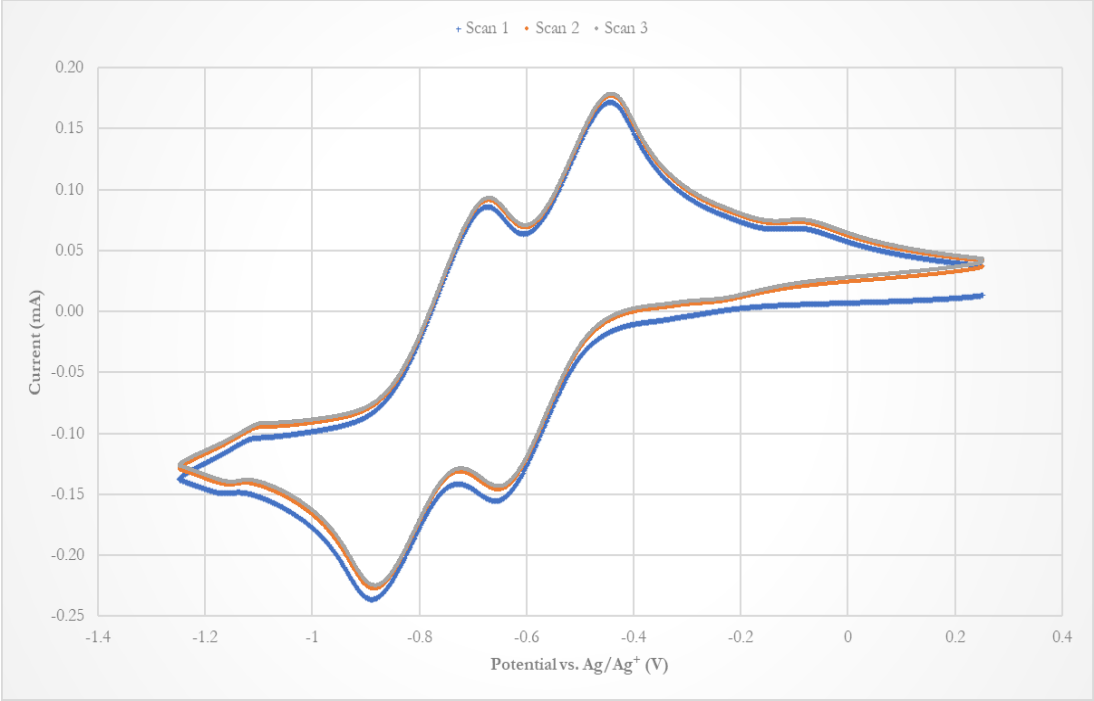

Figure 22. Cyclic voltammetry of $\mathbf{6}^{2+}$. 0.01 M in MeCN; 0.100 M $LiBF_4$; 100 mV/s; scans 1-3 shown.

Conclusions

Of the asymmetric di-pyridinium carbonyls, only compound $\mathbf{5}^{2+}$ has any sort of reversible redox activity at either event. The symmetric isomers are significantly more reversible in their redox chemistry, specifically, **[1^{2+}]2OTf** which has two reversible redox events under CV conditions. It may be possible to further stabilize this molecule by functionalizing the second ortho position. Compound $\mathbf{6}^{2+}$ was expected to have the most favorable electronic profile based on the stabilizing ability of an electron withdrawing group but was found to have a non-reversible second redox event. Due to the direct contradiction of our expectation and our experimental data, computational studies were needed to attempt to understand this observation.

Experimental

General considerations

2-bromopyridine was purchased from Alfa Aesar and used as received. 3-bromopyridine was purchased from Matrix Scientific and used as received. 4-bromopyridine hydrochloride was purchased from Alfa Aesar and used as received. 2-cyanopyridine was purchased from Acros Organics and used as received. 3-cyanopyridine was purchased from Alfa Aesar and used as received. 4-cyanopyridine was purchased from Alfa Aesar and used as received. Di-2-pyridyl methanone was purchased from Alfa Aesar and used as received. n-Butyl lithium was purchased from Alfa Aesar and used as received. Trimethyloxonium tetrafluoroborate was purchased from Alfa Aesar and purified in a nitrogen filled glovebox by rinsing with 5 mL of dry DCM twice, followed by 5 mL of dry diethyl ether, and filtered to obtain the white crystalline compound.

All dry solvents were dried and distilled under nitrogen before degassing and use.

All cyclic voltammetry measurements were made on a CH Instruments Model 600D Series Electrochemical Analyzer/Workstation in a nitrogen filled glovebox using dried and degassed solvents. These measurements were made using Ag/Ag+ reference from $AgNO_3$. $LiBF_4$ (0.1 M) was used as the supporting electrolyte.

All air-sensitive chemistry was carried out in a nitrogen filled glovebox or on a dry Schlenk line under nitrogen.

Nuclear magnetic resonance spectra were obtained on a Bruker Avance 400 MHz instrument or Bruker Avance 500 MHz instrument. Instrument used is noted with the given data. Deuterated solvents were obtained from Cambridge Isotopes and dried on molecular sieves for samples that were not air-sensitive. Air-sensitive NMR samples were prepared with deuterated solvents which had been dried appropriately, distilled, and degassed.

$[1^{2+}]2OTf^-$

Methyl triflate (0.410 mL, 0.5945 g, 3.62 mmol) was added dropwise to a cooled solution of di-2-pyridyl methanone (280.0 mg, 1.52 mmol) in dry DCM (20 mL) and was allowed to stir overnight in a nitrogen-filled glovebox, resulting in the formation of a white solid. The solid was isolated by vacuum filtration, washed with dry DCM (2 x 5 mL), and dried under vacuum to afford **$[1^{2+}]2OTf^-$** as a white powder (660.0 mg, 84.8% yield). mp. 182.0 – 183.5 °C. ^{1}H NMR (500 MHz, CD_3CN) δ 9.09 – 8.93 (m, 2H), 8.72 (td, *J* = 7.9, 0.9 Hz, 2H), 8.40 – 8.26 (m, 4H), 4.49 (s, 6H). ^{19}F NMR (376 MHz, CD_3CN) δ -79.32 (s).

$[1^{2+}]2BF_4^-$

In a nitrogen filled glovebox, trimethyloxonium tetrafluoroborate (260.1 mg, 1.76 mmol) was suspended in dry DCM (5 mL) in a 20 mL scintillation vial with rapid stirring. Di-2-pyridyl methanone (162.6 mg, 0.88 mmol) in dry DCM (5 mL) was added all at once and stirred at room temperature for 7 hours. The solution was filtered and washed with dry DCM (2 x 5 mL) to afford **$[1^{2+}]2BF_4^-$** as a tan powder (341.2 mg, 87.8% yield). mp. 262.4 °C (dec). ^{1}H NMR (400 MHz, CD_3CN): δ 9.01 (d, *J* = 5.9 Hz, 1H), 8.72 (tdd, *J* = 1.8, 1.3, 0.4 Hz, 1H), 8.33 (dd, *J* = 8.0, 5.5 Hz, 2H), 4.49 (s, 3H). ^{19}F NMR (376 MHz, CD_3CN): δ -151.68 (s). ^{11}B NMR (128 MHz, CD_3CN) δ -1.28 (s).

2

A schlenk flask under N_2 was charged with 1.7 mL of nBuLi (2.6 M in hexanes, 1.5 eq) and cooled to -78.0°C. 2-bromopyridine (0.29 mL, 0.4739 g, 3 mmol) in 15 mL of dry diethyl ether was added dropwise and stirred for 20 minutes. During the reaction, the clear, pale yellow solution took on a bright orange color. Methyl nicotinate (1.21 eq) in 10 mL of dry diethyl ether was then added dropwise to cold solution. The reaction mixture was stirred, cold, for 2 hours and subsequently quenched with 10 mL of saturated aqueous NH_4Cl and

washed twice with 10 mL H_2O. The solution was then dried over $MgSO_4$ and filtered. The orange solution was concentrated under vacuum to give a brown oil, which was then purified by column chromatography (80:20 EtOAc/Hexanes). The collected pale-yellow oil was dissolved in minimal EtOAc and precipitated in ether then left to recrystallize in a freezer for 48 hours. The resulting tan crystals were collected by vacuum filtration. (275.0 mg, 49.8% yield). ^{1}H NMR (400 MHz, CD_3CN) δ 9.19 (dd, *J* = 2.2, 0.9 Hz, 1H), 8.77 (dd, *J* = 4.8, 1.7 Hz, 1H), 8.71 (ddd, *J* = 4.8, 1.7, 1.0 Hz, 1H), 8.37 (ddd, *J* = 8.0, 2.2, 1.7 Hz, 1H), 8.17 – 8.06 (m, 1H), 8.06 – 7.95 (m, 1H), 7.62 (ddd, *J* = 7.6, 4.8, 1.3 Hz, 1H), 7.49 (ddd, *J* = 8.0, 4.8, 0.9 Hz, 1H).

2^{2+}

Methyl triflate (0.410 mL, 0.5945 g, 3.62 mmol) was added dropwise to a cooled solution of **2** (278.0 mg, 1.5 mmol) in dry DCM (20 mL) and was stirred overnight in a nitrogen-filled glovebox, resulting in the formation of a white solid. The solid was isolated by vacuum filtration, washed with dry DCM (2 x 5 mL), and dried under vacuum to afford **2^{2+}** as a white powder (760.0 mg, 99.4% yield). mp. 123.3-124.7°C. ^{1}H NMR (400 MHz, CD_3CN) δ 9.18 – 9.14 (m, 1H), 8.99 – 8.89 (m, 3H), 8.73 (tdd, *J* = 8.0, 1.4, 0.5 Hz, 1H), 8.27 (ddt, *J* = 12.2, 8.0, 3.6 Hz, 3H), 4.41 (s, 3H), 4.39 (s, 3H). ^{13}C NMR (101 MHz, CD_3CN) δ 183.96 (s), 151.08 (s), 150.72 (s), 149.00 (s), 148.08 (s), 147.25 (s), 134.82 (s), 131.85 (s), 131.20 (s), 129.55 (s), 55.27 (s), 49.93 (s), 48.75 (s). ^{19}F NMR (376 MHz, CD_3CN) δ -79.33 (s).

3

A schlenk flask under N_2 was charged with 8 mL of nBuLi (2.6 M in hexanes, 20.8 mmol) and cooled to -78.0°C. 2-bromopyridine (1.4 mL, 2.3198 g, 14.7 mmol) in 10 mL of dry diethyl ether was added dropwise and stirred for 30 minutes. During the reaction, the translucent pale yellow solution took on a bright orange color. 4-cyanopyridine (1.4595 g, 14.0 mmol) in

35 mL of dry diethyl ether was then added dropwise to cold solution. The solution turned to a deep burgundy upon completion of the addition. The reaction mixture was stirred, cold, for 2 hours and subsequently quenched with 20 mL of H_2O at which time the solution became a yellow-orange color. The reaction was warmed to room temperature, and then extracted with dilute aqueous H_2SO_4 (10%, 3 x 15 mL), which initially caused the solution to turn dark-brown. The combined aqueous layers were briefly heated to remove any ethereal solution. The solution was then neutralized with 2 M NaOH; upon neutralization, the orange acid washes precipitated a yellow powder. This neutralized solution was then extracted with DCM (3 x 20 mL), dried over $MgSO_4$, and filtered. The orange solution was concentrated under vacuum to yield a yellow solid, which was then dissolved in minimal DCM and precipitated in pentane to give a tan solid (414.6 mg, 32.1% yield). mp. 122.1 – 122.6 °C. ^{1}H NMR (400 MHz, $CDCl_3$) δ 8.86 – 8.82 (m, 2H), 8.76 (ddd, J = 4.8, 1.7, 0.9 Hz, 1H), 8.20 – 8.16 (m, 1H), 8.01 – 7.95 (m, 1H), 7.95 – 7.90 (m, 2H), 7.57 (ddd, J = 7.6, 4.8, 1.2 Hz, 1H). ^{13}C NMR (126 MHz, CD_3CN) δ 194.14 (s), 154.47 (s), 151.00 (s), 149.82 (s), 138.60 (s), 128.37 (s), 125.23 (s), 124.61 (s).

5

A schlenk flask under N_2 was charged with 1.6 mL of nBuLi (2.2 M in hexanes, 3.52 mmol) and cooled to -78.0°C. 3-bromopyridine (0.22 mL, 0.3608 g, 2.28 mmol) was dissolved in 6 mL of dry diethyl ether, added dropwise to the cold solution, then stirred for 30 minutes. 4-cyanopyridine (248.8 mg, 2.38 mmol) was dissolved in 6 mL of dry diethyl ether and added dropwise to the solution. Immediately upon addition of the 4-cyanopyridine, a color change to dark red was observed. The reaction was allowed to proceed for 2 hours at -78.0°C, at which time it was quenched with 10 mL of H_2O and warmed to room temperature. The aqueous layer was removed and the organic layer was washed with dilute aqueous H_2SO_4 (10%, 3 x 6 mL). The combined acid washes and aqueous layer were heated to remove residual ether

and then neutralized with 2 M aqueous NaOH solution. After neutralization, the solution was extracted with dry DCM (3 x 15 mL), dried over $MgSO_4$, filtered, and concentrated under vacuum. The recovered yellow solid was dissolved in minimal DCM and precipitated in hexane to obtain an egg-shell white powder (93.5 mg, 22.2% yield). ^{1}H NMR (500 MHz, CD_3CN): δ 8.95 (dd, *J* = 2.3, 0.8 Hz, 1H), 8.83 (dd, *J* = 4.9, 1.7 Hz, 1H), 8.81 (dd, *J* = 4.3, 1.7 Hz, 2H), 8.13 (ddd, *J* = 7.9, 2.3, 1.7 Hz, 1H), 7.62 (dd, *J* = 4.3, 1.7 Hz, 2H), 7.53 (ddd, *J* = 8.0, 4.8, 0.9 Hz, 1H). ^{13}C NMR (126 MHz, CD_3CN): δ 195.16 (s), 154.61 (s), 151.72 (s), 151.53 (s), 144.36 (s), 138.14 (s), 132.69 (s), 124.56 (s), 123.63 (s).

5^{2+}

Compound **5** (93.5 mg, 0.52 mmol) was dissolved in 5 mL of dry DCM in a N_2 filled glovebox and cooled to -20°C. Methyl triflate (0.14 mL, 0.203 g, 1.24 mmol) was added dropwise to the solution with rapid stirring. Immediate precipitation of a tan powder was observed. After 12 hours, the precipitate was collected by vacuum filtration and washed with dry DCM (2 x 5 mL) to collect a white powder (224.0 mg, 86.2% yield). mp. 149.2 – 151.0°C. ^{1}H NMR (500 MHz, CD_3CN): δ 9.07 (s, 1H), 8.91 (t, *J* = 6.8 Hz, 3H), 8.79 (d, *J* = 8.2 Hz, 1H), 8.27 (d, *J* = 6.2 Hz, 2H), 8.25 – 8.19 (m, 1H), 4.44 (s, 3H), 4.41 (s, 3H). ^{19}F NMR (376 MHz, CD_3CN): δ -79.34 (s).

6

H_2O (20 mL), 1 M NaOH (aq, 40 mL), and dry diethyl ether (40 mL) were cooled in an ice bath to 0°C**.** 4-bromopyridine hydrochloride (3.0551 g, 15.71 mmol) was dissolved in the cooled NaOH solution and then extracted with the cold diethyl ether (2 x 20 mL). Note: it is of the utmost importance that the 4-bromopyridine hydrogen chloride is not permitted to reach a temperature above 5°C. The combined ether layers were then rinsed with the cold H_2O (2 x 10 mL), dried over $MgSO_4$, filtered and concentrated under vacuum slowly to a

volume of approximately 5 mL. Concurrently, a schlenk flask under N_2 was charged with 8.5 mL of nBuLi (2.6 M in hexanes, 22.1 mmol) and cooled to -78.0°C. Fresh dry diethyl ether (8 mL) was added to the 4-bromopyridine oil and then added dropwise to the cold nBuLi. The reaction mixture was stirred for 40 minutes at -78.0°C, at which time a solution of 4-cyanopyridine (1.8136 g, 17.42 mmol) in 30 mL of dry diethyl ether was added dropwise to the solution. The reaction was stirred cold for 55 minutes then moved to an ice bath and quenched with 30 mL H_2O. The resulting mixture was extracted with dilute H_2SO_4 (aq, 10%, 2 x 20 mL) and combined aqueous layers were heated gently to remove any ether residue. The acidic washes were then neutralized with 1 M NaOH, approximately 104 mL, at which point a yellow precipitate was observed. This was extracted with DCM (4 x 25 mL), dried over $MgSO_4$, filtered, and concentrated under vacuum. The resulting oil was dissolved in approximately 3 mL of DCM and precipitated in 40 mL of dry pentane and left in a -4°C freezer overnight. Formation of dark orange crystals was observed, and the crystals were separated by filtration and washed with copious amounts of pentane. The solid collected was subsequently dissolved in 1 mL of $CDCl_3$ and precipitated in 15 mL of dry pentane to yield the pure product as a pale orange powder (382.2 mg, 13.2% yield). mp. 141.6 – 142.3°C. ^{1}H NMR (500 MHz, $CDCl_3$): δ 8.87 (dd, J = 4.4, 1.7 Hz, 4H), 7.61 (dd, J = 4.4, 1.7 Hz, 4H). ^{13}C NMR (126 MHz, $CDCl_3$): δ 194.05 (s), 150.80 (s), 142.32 (s), 122.68 (s).

6^{2+}

Compound **6** (109.7 mg, 0.60 mmol) was dissolved in 6 mL of dry DCM in a nitrogen filled glovebox. Methyl triflate (0.15 mL, 0.217 g, 1.33 mmol) was added dropwise while stirring at -20°C and subsequently stirred for 22 hours. Upon addition of methyl triflate to the solution, the solution underwent a change in color from amber to dark brown; as more precipitate formed, the solution took on a red color and a tan powder was recovered (133.3

mg, 43.7% yield). ^{1}H NMR (400 MHz, CD_3CN) δ 8.93 (d, J = 6.4 Hz, 2H), 8.26 (d, J = 5.6 Hz, 2H), 4.44 (s, 3H). ^{13}C NMR (126 MHz, CD_3CN): δ 189.23 (s), 148.44 (s), 148.08 (t, J = 8.9 Hz), 128.68 (s), 123.37 (s), 120.82 (s), 50.01 (s). ^{19}F NMR (471 MHz, CD_3CN): δ -79.30 (s).

III. COMPUTATIONAL STUDY OF MONO-PYRIDYL KETONE RADICALS

Introduction

As previously stated, the mono-pyridinium systems studied by Sevov *et. al* were very influential in the development of the bulk of this thesis. Because of the observed higher reversibility and stability of **[1^{2+}]2OTf**, we wanted to see if there was any discernible correlation between these mono-pyridyl ketone radicals systems' substituents and the reactivity with triplet oxygen as with the systems studied by Mahoney and if there was a difference in the ortho and para substituted mono-pyridyl ketone radical compounds.[60] Mahoney's Hammett analysis clearly indicates that the more electron withdrawing a substituent is the more capable it is of stabilizing a radical species. An important note regarding his analysis is that the reported enthalpy of reaction for each of these reactions with triplet oxygen is more in line with what would be expected for a weak association rather than a formal bond forming event. Regardless, the model seems to hold up given the stability of up to two years in atmosphere for Bertrand's compounds.

It may be of interest to note that Hammett analysis has been studied for the redox properties of mono-pyridinium compounds previously.[73] Hammett analysis comparing electron withdrawing character of substituents on the phenyl of a para-benzoyl pyridinium compounds, shown in ***Figure 23***, with the potential of the first reduction event was found to have a high correlation. As the electron withdrawing character of the substituent increases, the $E_{1/2}$ of the first reduction event is cathodically shifted.

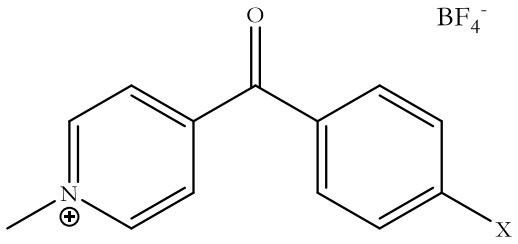

Figure 23. p-(4-substituted-benzoyl)-N-methyl pyridinium. X = OMe, Me, H, SMe, Br, CCH, CHO, NO_2, $^+S(CH_3)_2$.

The literature provides a sound basis for studying the reactivity of acylated mono-pyridyl ketone radicals, shown in ***Figure 24***, with triplet oxygen.

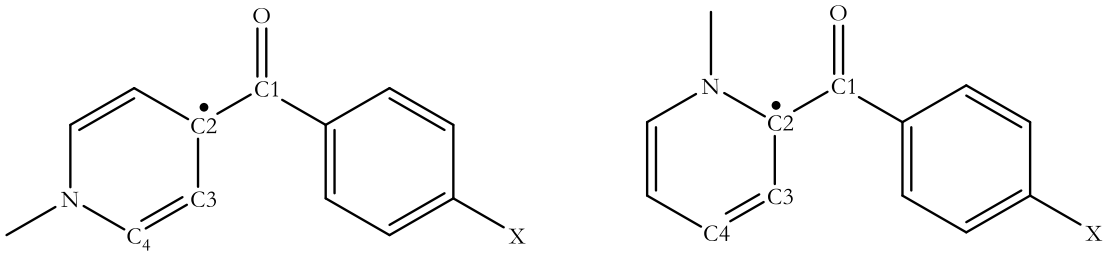

7a-l **8a-l**

Figure 24. Mono-pyridyl ketone radicals for Hammett analysis.

Table 1. Substituent identity of **7a-l** and **8a-l**.

Compound (7 or 8)	Substituent, X
a	NMe_2
b	NH_2
c	OH
d	OMe
e	Me
f	H
g	SMe
h	Br
i	CHO
j	$COCH_3$
k	CN
l	NO_2

By using DFT to calculate the enthalpy of the mono-pyridyl ketone radicals, triplet oxygen, and the oxygen adducts of the mono-pyridyl ketones, we can approximate the effect of substituents on the stability of our proposed radical species.

Para-functionalized mono-pyridyl ketone radicals

Based on Bertrand's work and our operating assumption that the para-substituted system could be treated as a remote NHC, we began density functional theory calculations on this suite of molecules. Using the hybrid (U)B3LYP/6-311++g(*) level of theory, optimizations were run for a large collection of mono-pyridyl ketone radical compounds.

A correlation between Hammett parameter (σ_p) and the ratio of Mulliken spin density on the carbon ortho to the nitrogen heteroatom and the Mulliken spin density on the oxygen of the carbonyl was not obtained (***Figure 25***.) While that ratio wasn't particularly high, it is worth mentioning that there was consistently larger absolute Mulliken spin density calculated for the carbon ortho to the heteroatom, C4, than there was at the para position, C2.

Table 2. Mulliken spin density at C2 and C4 positions of compounds **7a-l**.

Compound 7	C2 spin density	C4 spin density
a	-0.105	-0.735
b	0.144	-0.712
c	0.034	-0.679
d	0.236	-0.844
e	0.133	-0.819
f	-0.124	-0.521
g	0.243	-0.801
h	-0.024	-0.694
i	0.146	-0.829
j	0.125	-0.836
k	0.099	-0.806
l	0.036	-0.704

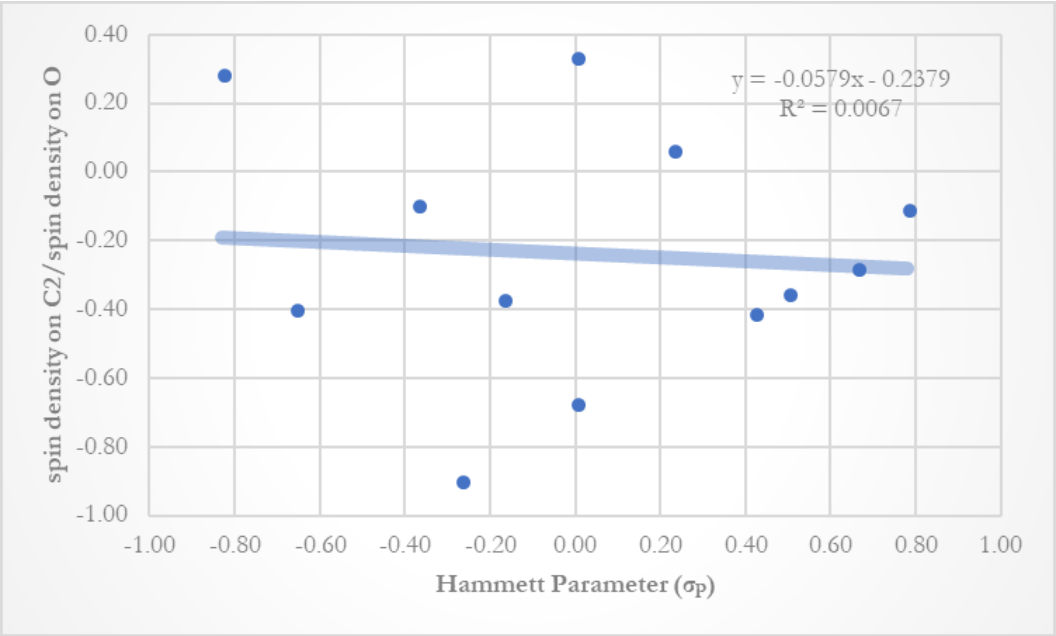

Figure 25. Comparison of Hammett parameter and Mulliken spin density ratio of C2/O in compounds **7a-l**.

At first glance, the enthalpies of reaction obtained seem to be quite small; however, the enthalpies reported by Bertrand are in a similar range and should probably be considered an association event rather than a bond forming event as indicated by the range of enthalpies (~5 kcal/mol to ~15 kcal/mol). Additionally, the geometry optimization files show a C-O bond length of typically somewhere between 2.7 and 2.9 Å which is much longer than would be expected if a bond was forming. Thermodynamic data was gathered from frequency calculations at the same level of theory as the optimizations and used to develop the Hammett analysis in ***Figure 26A***.

An anomalously low enthalpy of reaction was observed for **7l**. This could be indicative of a threshold of sorts with respect to the allowable electron withdrawing ability of the substituent in compounds **7a-l**. When the enthalpy of reaction for **7l** with triplet oxygen is removed from the Hammett analysis, as shown in ***Figure 26B***, the R^2 increases from 0.2711 to 0.9187, meaning that the nitro substituent is a significant outlier and should not be considered in part

of the general trend but should not be ignored in the full context of the study. As this analysis was completed to try and understand the poor reversibility of $\mathbf{6}^{2+}$, if a threshold for electron withdrawing character is indeed present in the para-acylated compounds **7**, it would explain why the incorporation of a cationic moiety such as para-(N-methyl)-pyridinium would possibly have such poor reversibility.

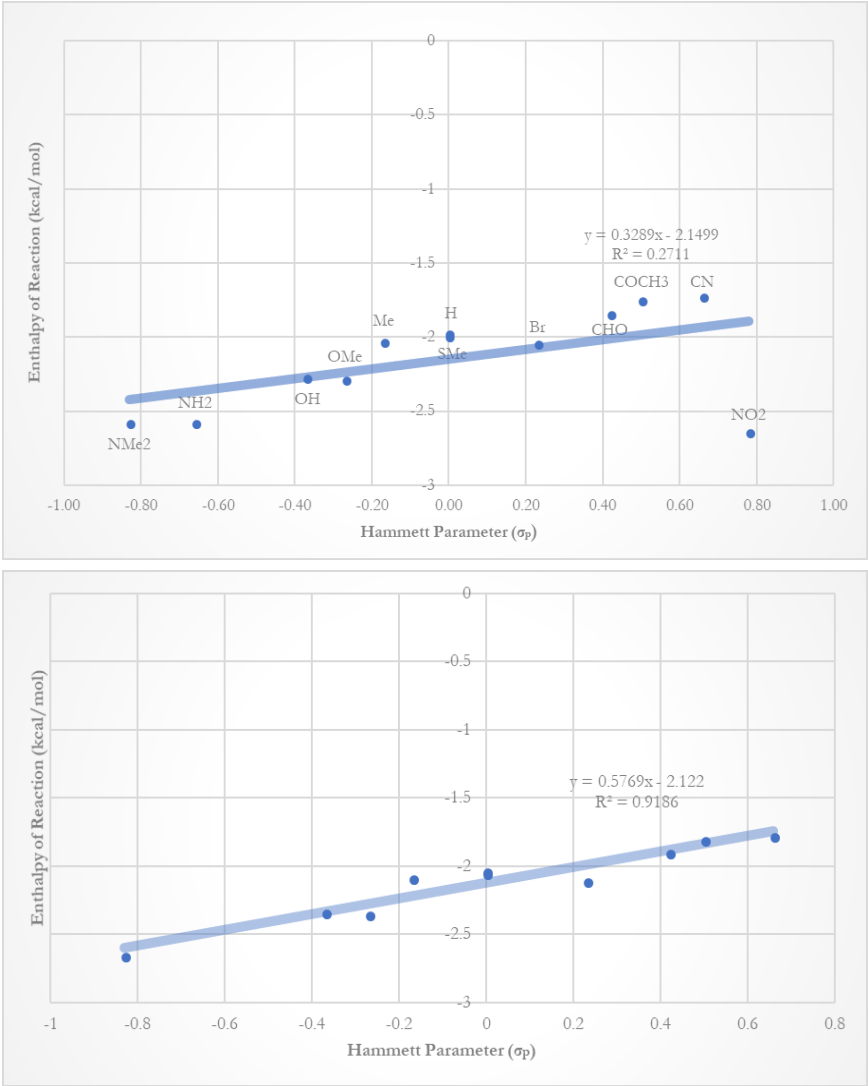

Figure 26. A) Shown top: Hammett Analysis of para-acylated mono-pyridyl ketone radical series, **7a-l**; B) Shown bottom: Hammett analysis of para-acylated mono-pyridyl ketone radical series, **7a-k**.

Ortho-functionalized mono-pyridyl ketone radicals

To further understand the observations and differences in $\mathbf{1}^{2+}$ and $\mathbf{6}^{2+}$ in terms of

reversibility of reduction and stability, the ortho-acylated derivatives were also studied. The substituents on the phenyl ring were the same as those tested on the para-functionalized pyridinium series, and all calculations were run at the same level of theory ((U)B3LYP/6-311++g(*)). A higher correlation in the Hammett analysis compared to the para-functionalized series was observed and can be seen in ***Figure 27***.

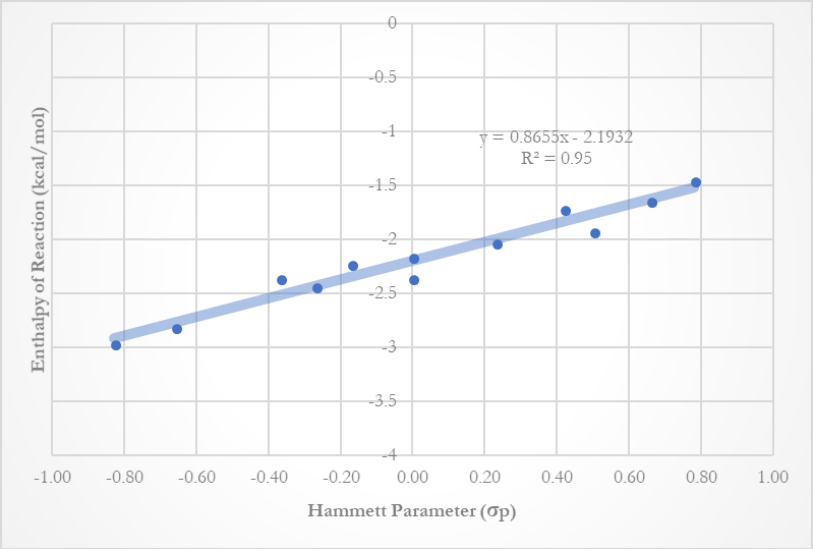

Figure 27. Hammett analysis of ortho-acylated mono-pyridyl ketone radical series **8a-l.**

Similar to the para-acylated series, **7a-l**, the enthalpy of reaction calculated is more in line with an association event rather than a formal bond making event. The C-O bond distance observed is less than that of the para-acylated series, which may be due to the dihedral angle at the studied position allowing for less steric hinderance and thusly a closer association of oxygen while still not formally bonding. Again, there is a difference in the Mulliken density at the carbon ortho to the heteroatom versus the para position (***Figure 28*** and ***Table 3***.)

With a Hammett analysis slope of 0.8655, it's clear that the ortho-acylated compounds are more strongly affected by the electronic properties of the substituent than the para-acylated isomers (slope of 0.5796 when **7l** is excluded). There is also reason to believe that increasing the electron withdrawing character of the substituent does not have a threshold before it decreases stability as is observed in the para-acylated isomers.

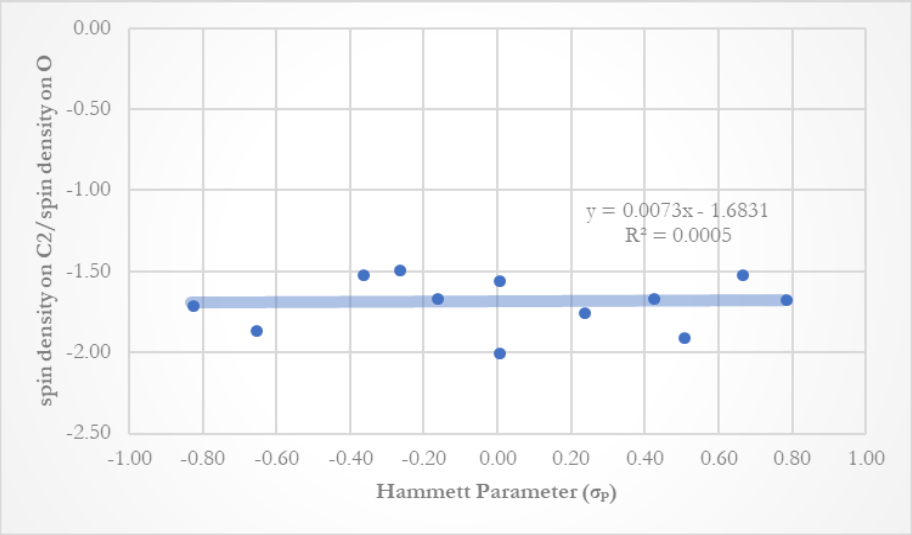

Figure 28. Comparison of Hammett parameter and Mulliken spin density ratio of C2/O in compounds **8a-l**.

Table 3. Mulliken spin density at C2 and C4 positions of compounds **8a-l**.

Compound 8	C2 spin density	C4 spin density
a	0.442	-0.307
b	0.479	-0.364
c	0.371	-0.285
d	0.379	-0.452
e	0.415	-0.409
f	0.499	-0.149
g	0.39	-0.471
h	0.433	-0.361
i	0.407	-0.388
j	0.47	-0.083
k	0.373	-0.348
l	0.404	-0.307

Conclusions

While the correlations of the para- and ortho-acylated compounds' Hammett parameters and enthalpy of reaction with triplet oxygen are not so markedly different, the higher dependence on electronic properties of substituents observed in the ortho-acylated mono-pyridyl ketone radical series offers some insight regarding Bertrand's observations and the electrochemical experimental observations in this thesis. The pattern observed here and by Bertrand indicates that increasing electron withdrawing properties of a substituent on an N-heterocyclic molecule induced preferred radical localization on the carbon ortho to the heteroatom. The radical homo-coupling through the ortho position of singly reduced para-substituted pyridinium compounds is known, and while the incorporation of the electron withdrawing group may stabilize the position, it clearly does not do so to a degree to prevent this radical coupling as evidenced by the experimental data collected on $\mathbf{6}^{2+}$. It is possible that modification to the ortho positions of $\mathbf{6}^{2+}$ may lead to drastically improved stability of this compound. These observations can also readily be applied to future potential systems of study, and functionalization of $\mathbf{1}^{2+}$ at the ortho position that is not bound to the carbonyl may even further stabilize the compound for use in redox flow batteries.

Experimental

All optimizations were carried out at the (U)B3LYP/6-311++g(*) level of theory, which was chosen based on previous literature, with tight convergence criteria.[60]

All frequency calculations were carried out at the same level of theory as the optimizations.

A scaling factor of 0.97 was applied to all thermodynamic data calculated and was chosen from the NIST database. A scaling factor for B3LYP/6-311++g(*) is not published, so the scaling factor of a similar level of theory was used.[74] B3LYP/6-311+g(3df,2pd) is similar to that used in these calculations, save an additional application of s functions.[75]

Calculations with a single imaginary frequency were confirmed to only have an imaginary frequency corresponding to the rotation of the methyl group at the alkylated nitrogen. No calculations had more than one imaginary frequency.

Table 4. Hammett analysis data for para-acylated mono-pyridyl ketone radicals.

Compound	Hammett Parameter of X	C-O bond length (Å)	dH reaction (kcal/mol)
7a	-0.83	2.75	-1.97
7b	-0.66	2.76	-2.03
7c	-0.37	2.76	-2.28
7d	-0.27	2.77	-1.99
7e	-0.17	2.89	-2.58
7f	0.00	2.79	-2.04
7g	0.00	2.89	-1.84
7h	0.23	2.79	-2.64
7i	0.42	2.80	-1.73
7j	0.50	2.88	-1.75
7k	0.66	2.81	-2.27
7l	0.78	2.82	-2.58

Table 5. Hammett analysis data for ortho-acylated mono-pyridyl ketone radicals.

Compound	Hammett Parameter of X	C-O bond length (Å)	dH reaction (kcal/mol)
8a	-0.83	2.62	-2.16
8b	-0.66	2.62	-2.23
8c	-0.37	2.65	-2.44
8d	-0.27	2.65	-2.36
8e	-0.17	2.67	-2.81
8f	0.00	2.68	-2.02
8g	0.00	2.66	-1.71
8h	0.23	2.69	-1.45
8i	0.42	2.72	-1.64
8j	0.50	2.71	-1.92
8k	0.66	2.72	-2.36
8l	0.78	2.74	-2.96

IV. SUMMARY AND FUTURE WORK

Asymmetric dipyridinium carbonyl species do not hold promise as materials in redox flow batteries. Compound $\mathbf{2}^{2+}$ does not undergo reversible redox events and couples to form several products upon reduction. Compound $\mathbf{3}^{2+}$ is not readily accessible, precluding incorporation into redox flow batteries. Compound $\mathbf{5}^{2+}$ undergoes one quasi-reversible redox event and one non-reversible event. This compound could possibly be functionalized to facilitate reversibility of one electronic process, but not both due to the presence of the meta-pyridinium moiety. The symmetric isomers are significantly more likely to be useful in the application of redox flow batteries. Specifically, $\mathbf{[1}^{2+}\mathbf{]2OTf}$ undergoes two reversible and discrete redox events under CV conditions. This molecule may be further modified to provide higher stability at the position ortho to the heteroatom by the functionalization of the secondary ortho position and incorporation of electron withdrawing moieties. Compound $\mathbf{6}^{2+}$ was expected to undergo two reversible redox events due to the stabilizing ability of an electron withdrawing group (the second cationic center), but was found to have a non-reversible second redox event. This may be due to radical homo-coupling through the ortho-position, which is well documented in singly reduced para-substituted pyridinium species.

Hammett analysis of ortho- and para-acylated mono-pyridyl ketone radical reactivity with triplet oxygen indicates that the incorporation of electron withdrawing groups has a much larger effect on the ortho-acylated isomers than the para-acylated isomers. This may indicate that the incorporation of an electron withdrawing moiety specifically stabilizes the position, with regard to radical stability, ortho to the heteroatom in pyridinium based molecules more so than the para.

There is still considerable work to be done to further explore the use of carbene derivatives as redox flow materials and to be done on poly-cationic systems such as the di-pyridinium

ketones. One of the major hurdles in redox flow batteries currently is the development of anolytes and catholytes that will not permeate the ionic membrane required to maintain charge. This issue is being worked at by polymer scientists from the perspective of creating smaller and smaller pore sizes in membranes, but that can only be so feasible before redox flow batteries begin to experience the same drawbacks in dendritic ion intercalation as their solid state counterparts. The alternative to making the pore sizes smaller is to make the electrochemically active materials larger. We have explored various aspects of literature surrounding poly-cationic pyridinium systems in the course of this work and believe that compounds containing dendritic or "star" structures with pyridinium moieties, such as ***Figure 29***, may be suitable for these purposes.[76]

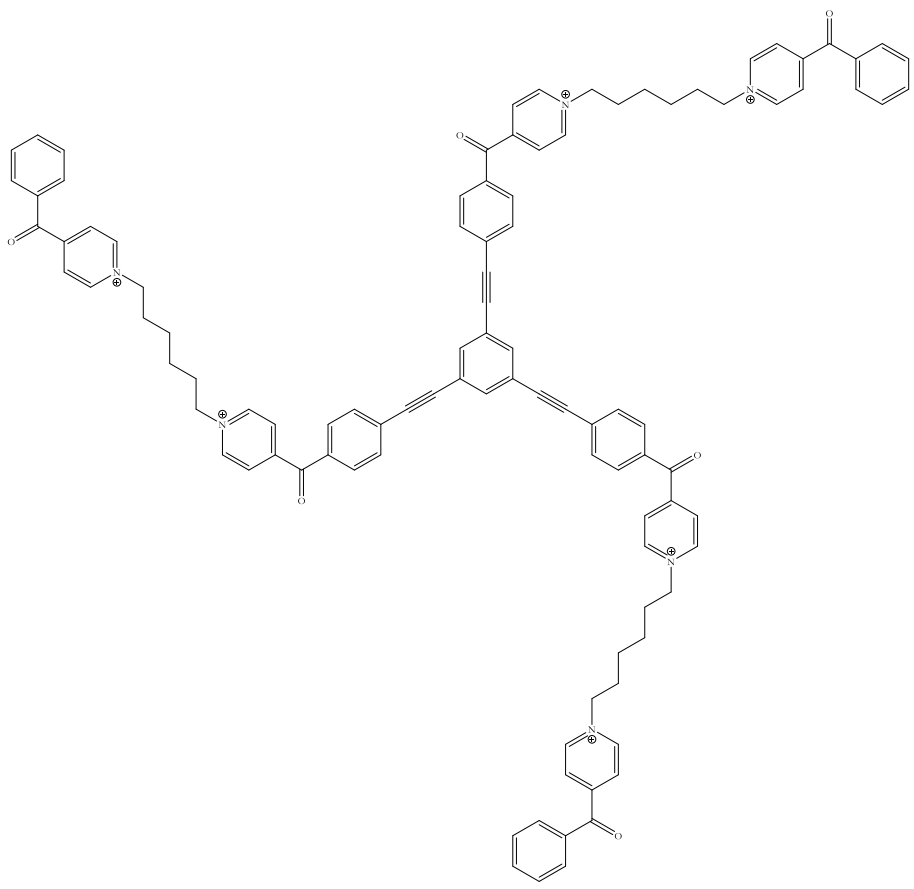

Figure 29. "Star" molecule that incorporates p-benzoyl pyridinium moiety.

Another avenue we are currently in the process of exploring is extending the aromatic length of molecules and substituents. Extension of an aromatic length decreases the HOMO/LUMO gap, which may influence the reversibility of single or multielectron processes. Further, by virtue of modifying the HOMO/LUMO energies, we expect that we can further tune the potential of reduction for our anolytes.

APPENDIX SECTION

[1^{2+}]2OTf ^{1}H NMR in CD_3CN

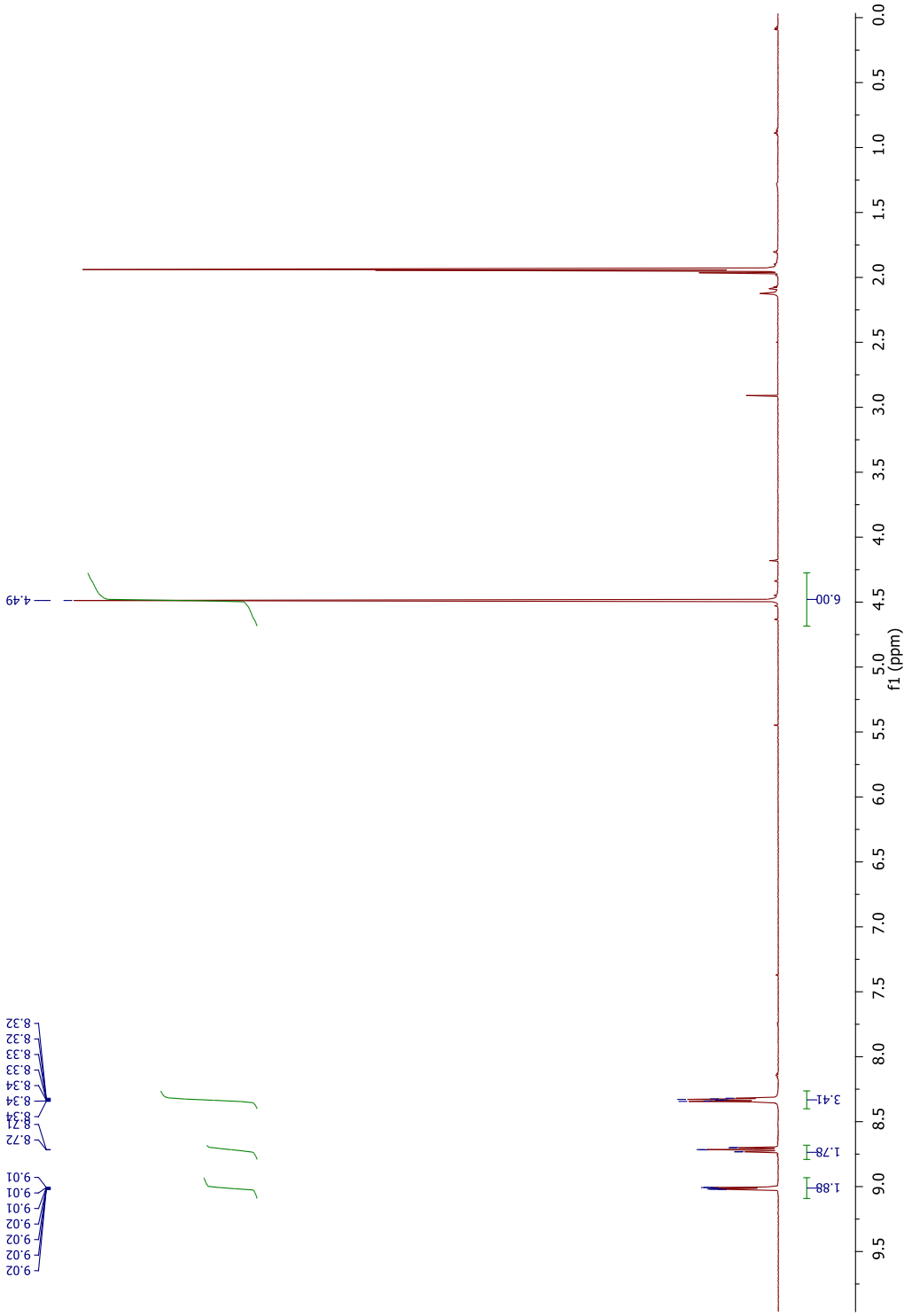

[1^{2+}]2OTf ^{19}F NMR in CD_3CN

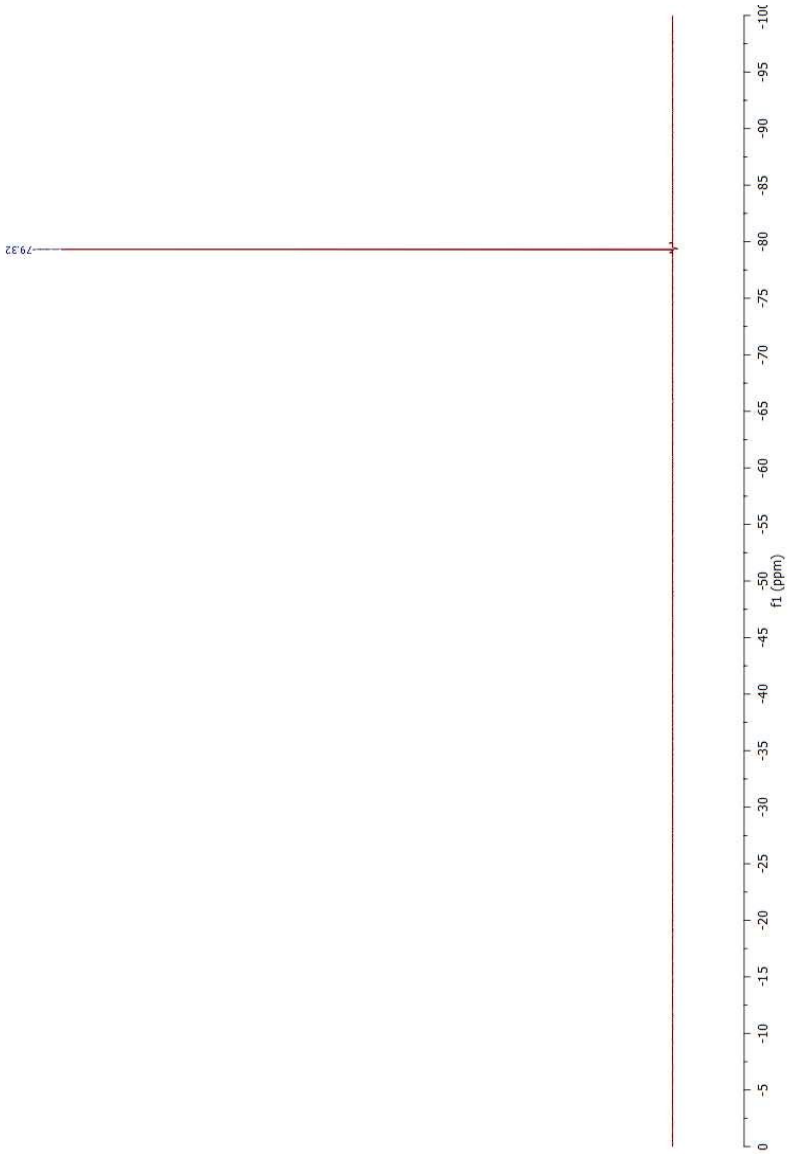

[1^{2+}]2BF_4^- ^{1}H NMR in CD_3CN

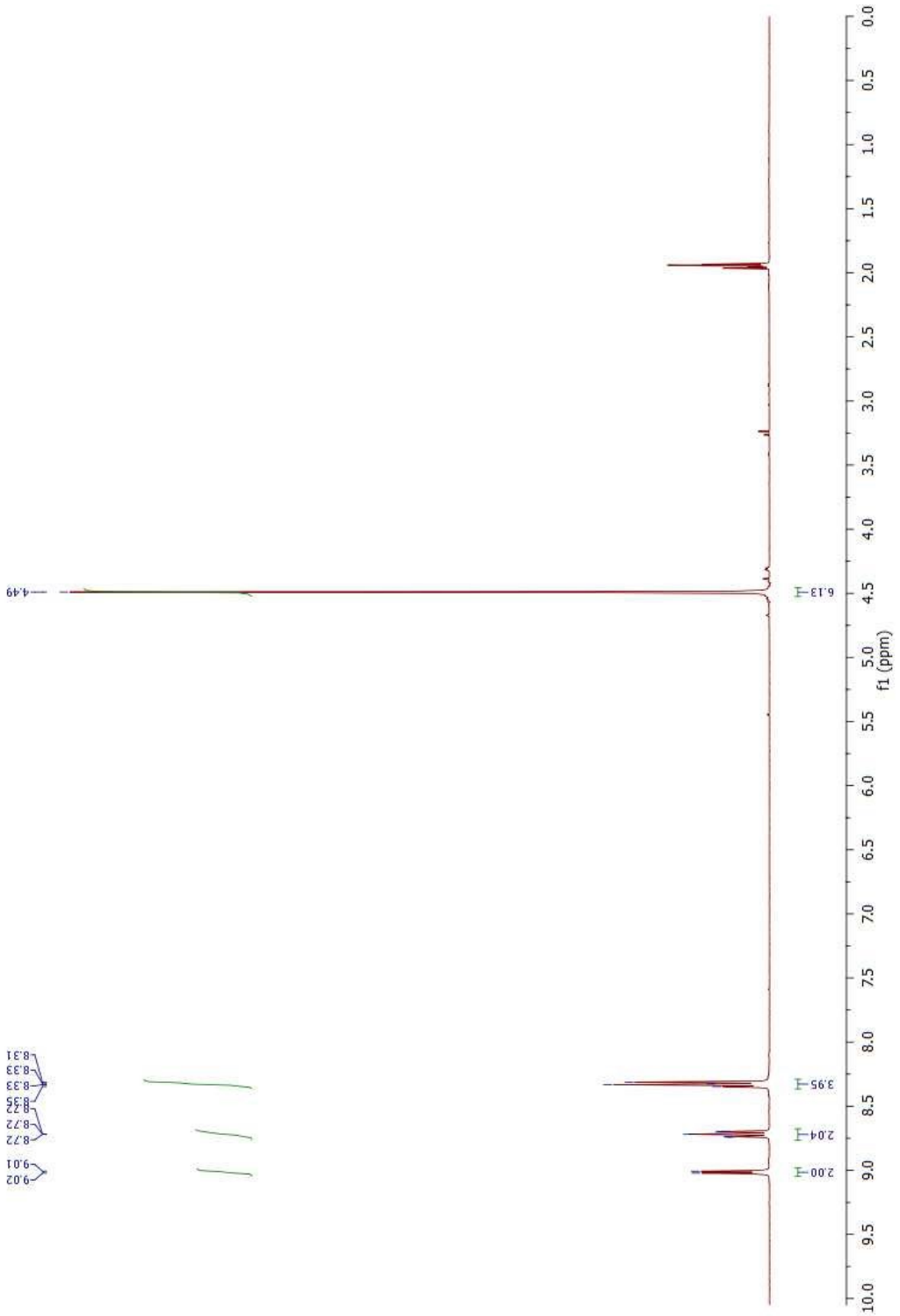

[1^{2+}]2BF$_4^-$ ^{19}F NMR in CD_3CN

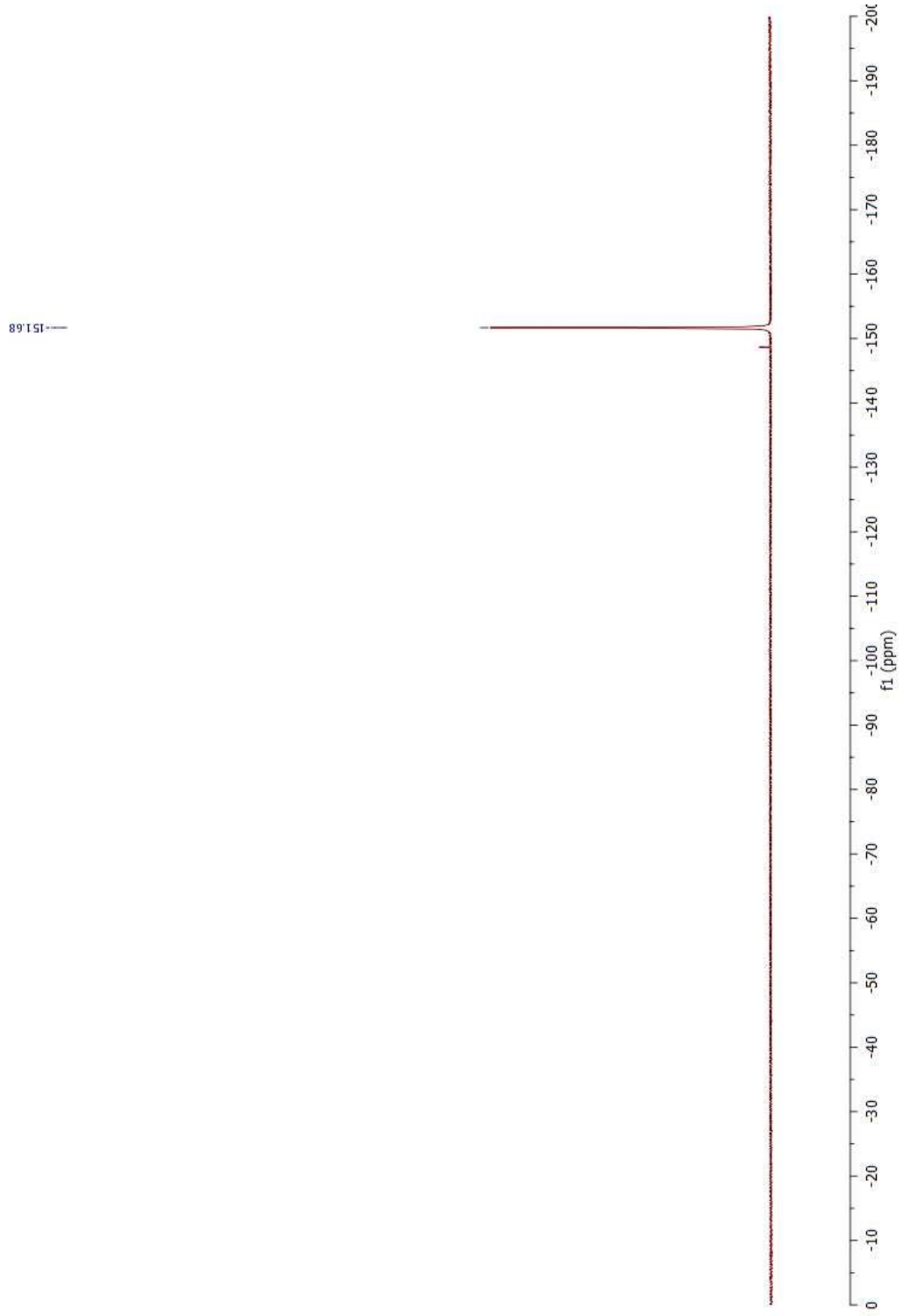

[1^{2+}]2BF_4^- ^{11}B NMR in CD_3CN

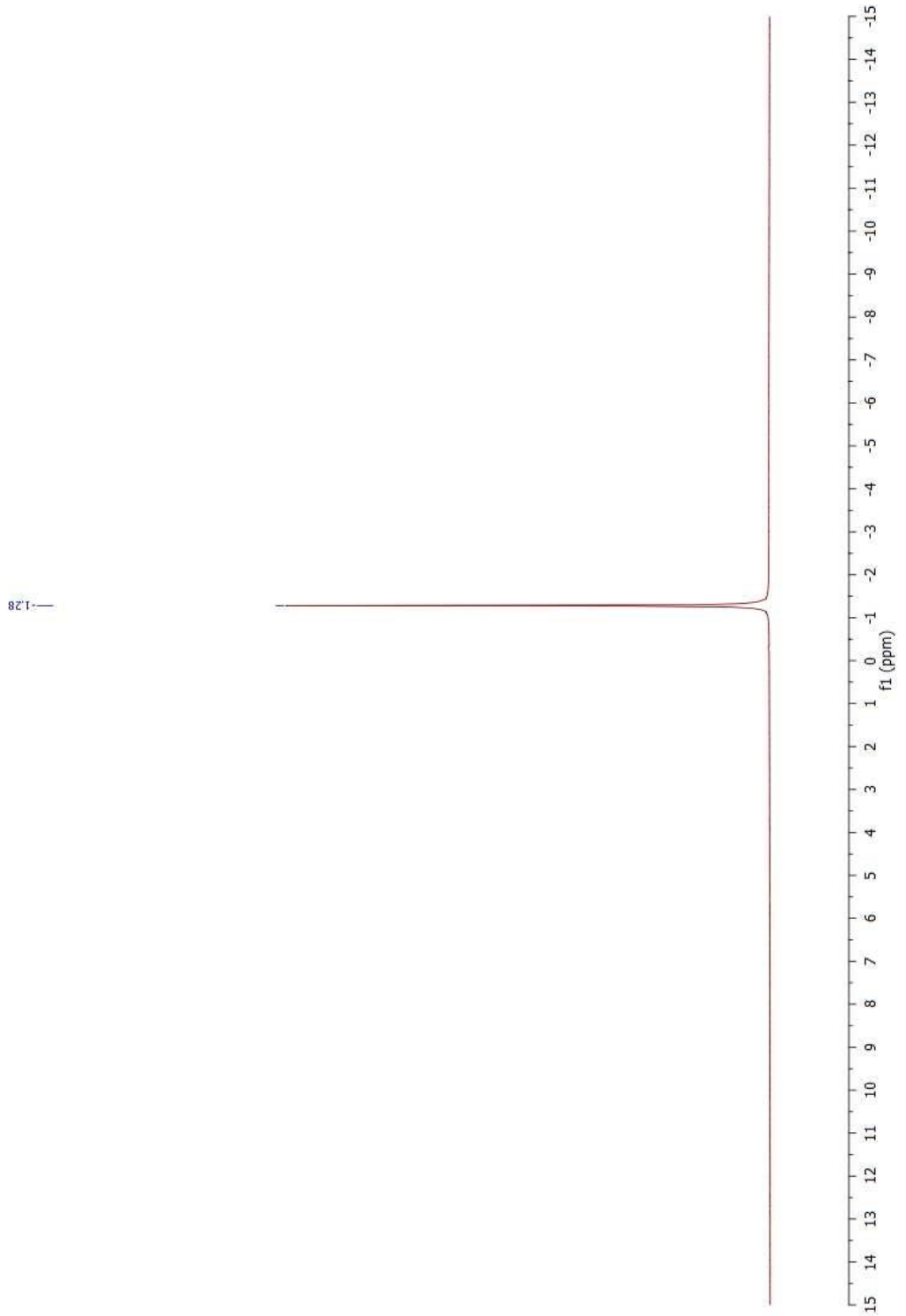

2 ^{1}H NMR in CD_3CN with acetone impurity

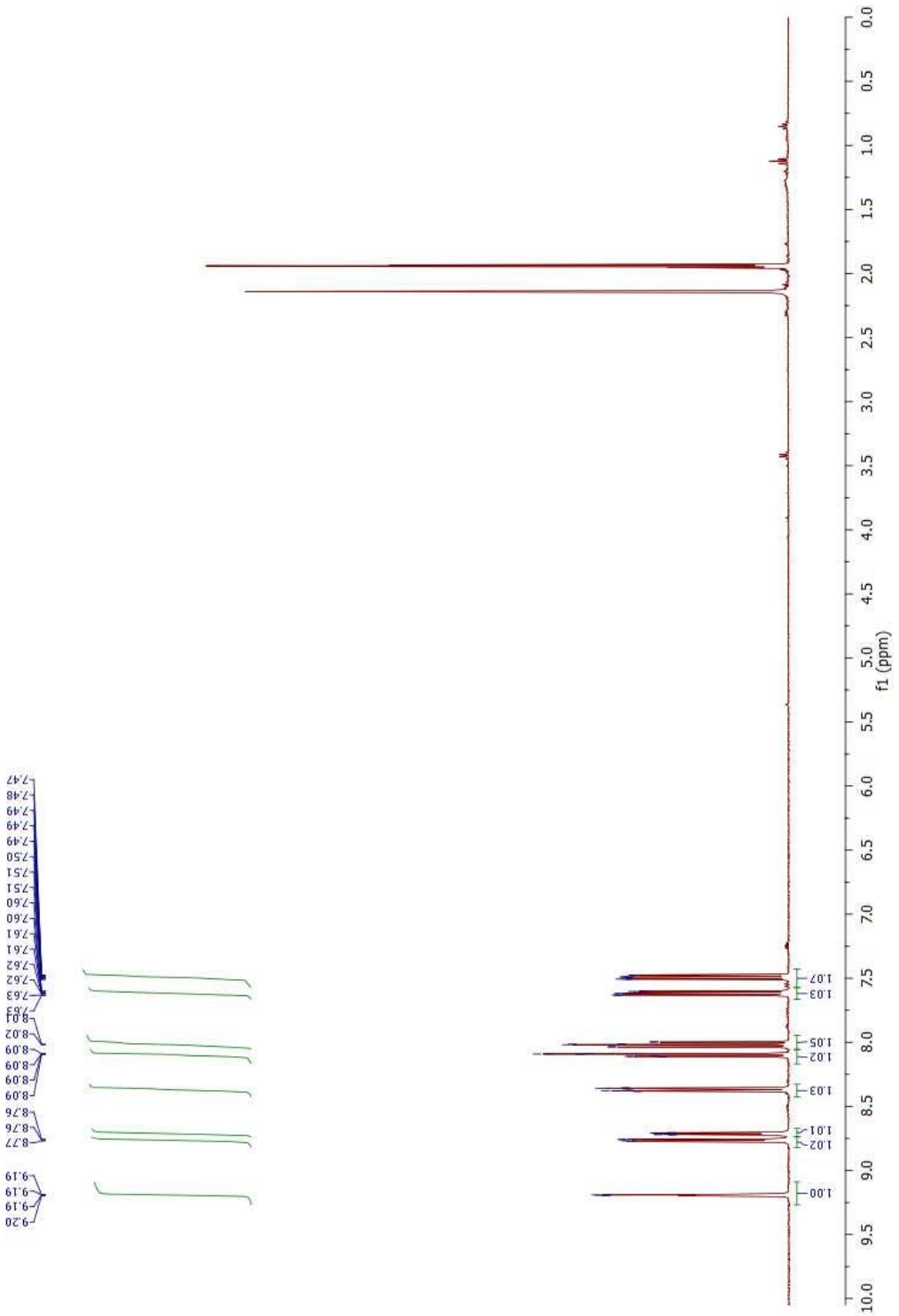

$\mathbf{2}^{2+}$ ^{1}H NMR in CD_3CN with DCM impurity

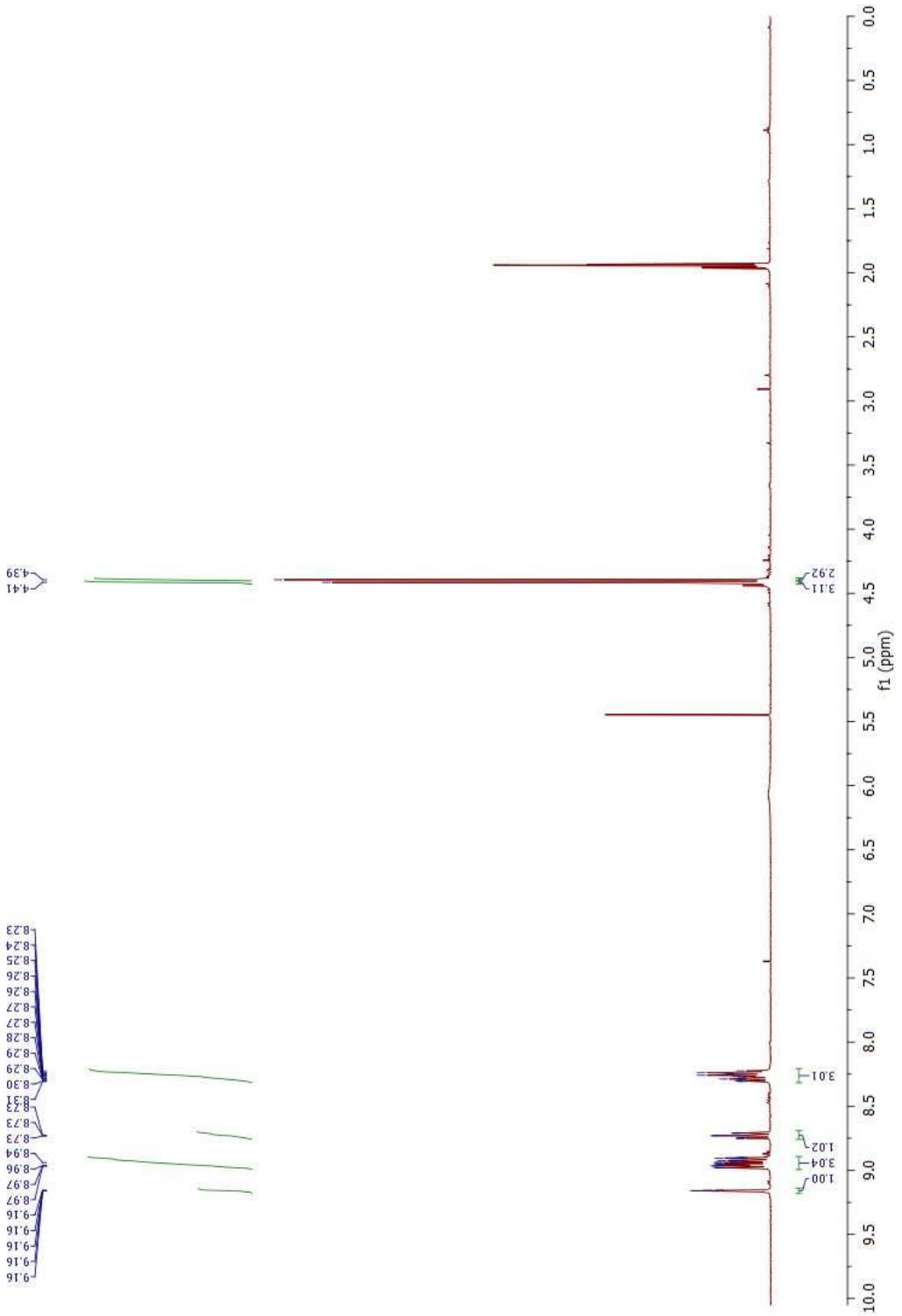

2^{2+} ^{13}C NMR in CD_3CN

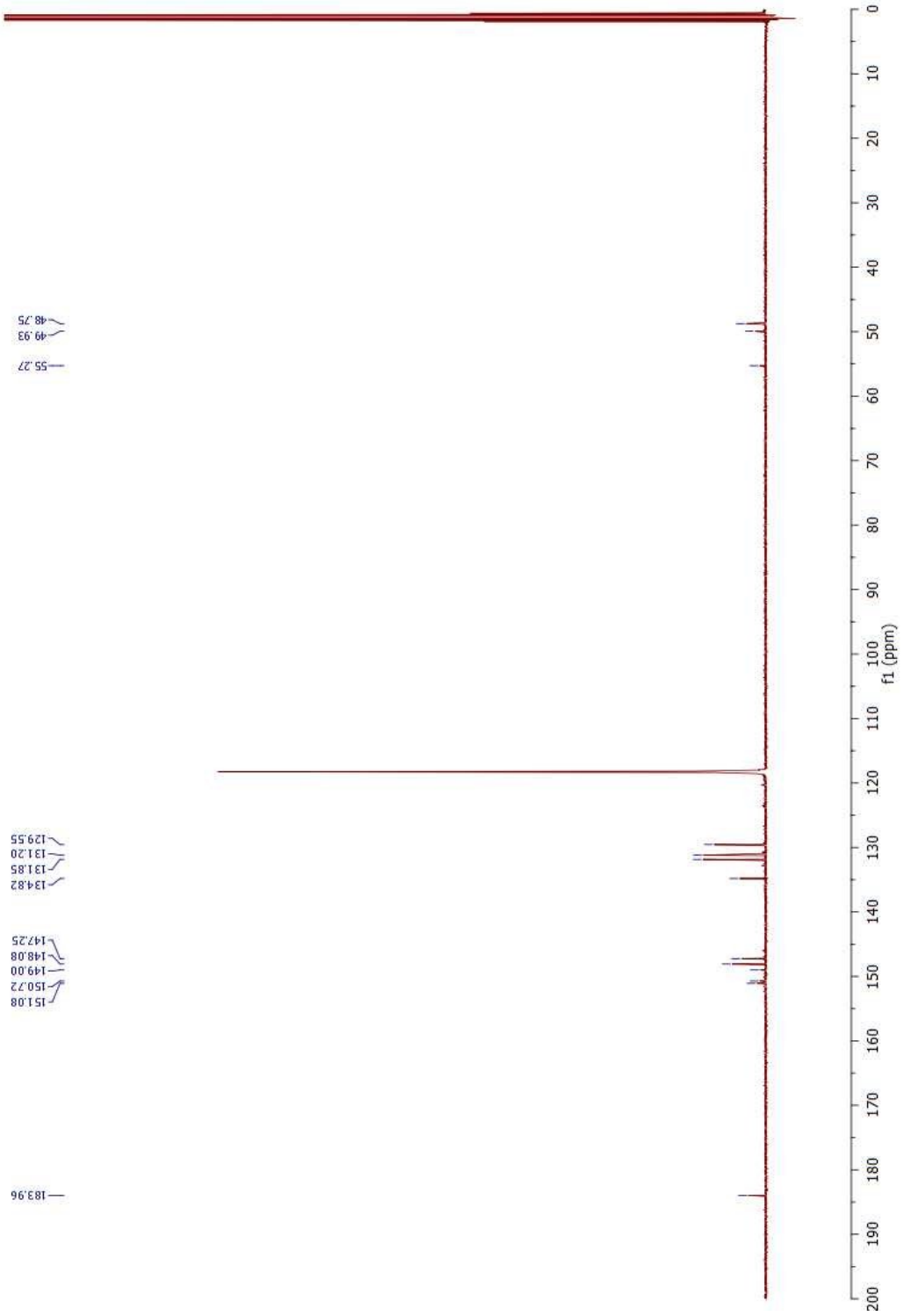

$\mathbf{2}^{2+}$ ^{19}F NMR in CD_3CN

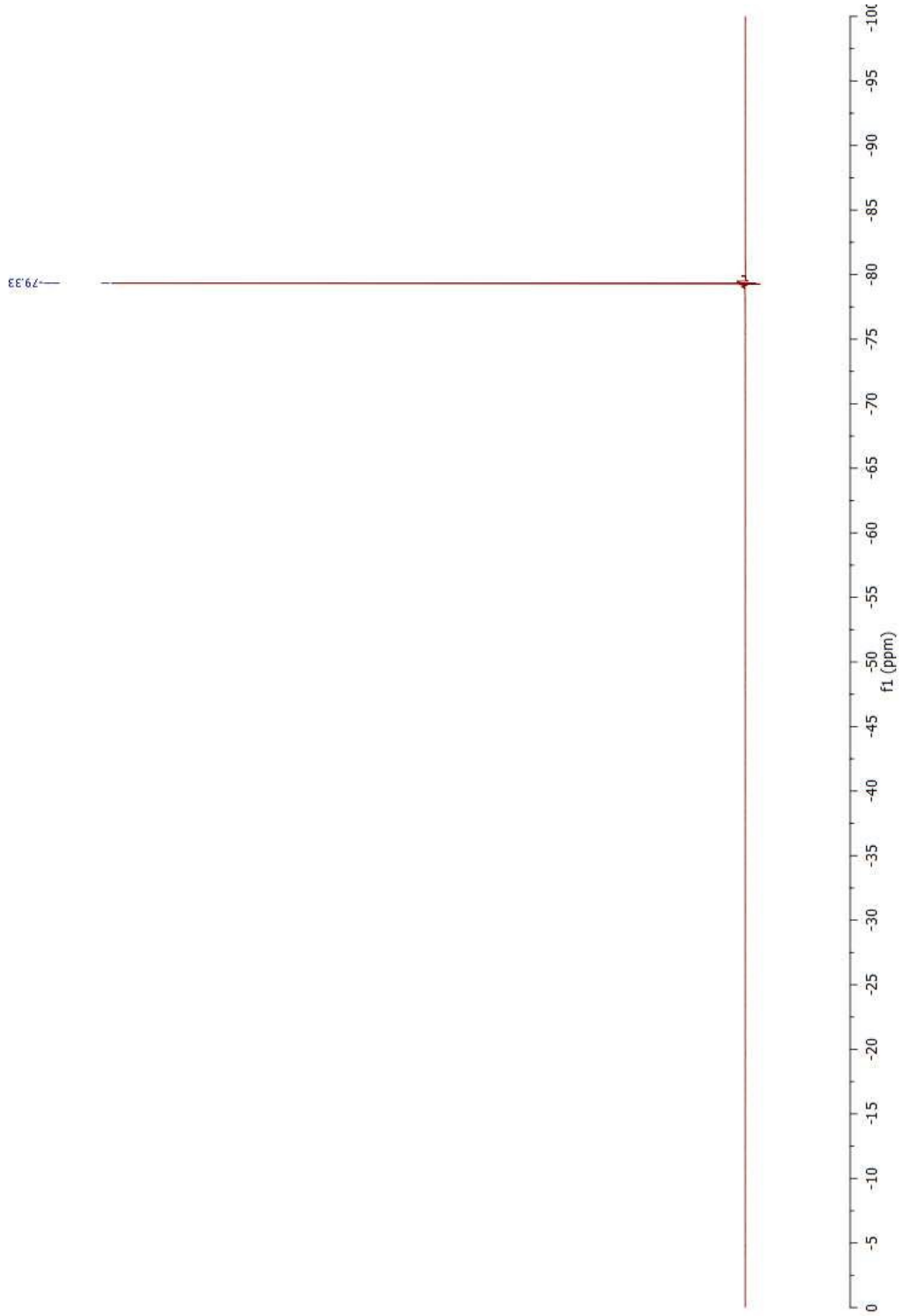

3 ^{1}H NMR in $CDCl_3$

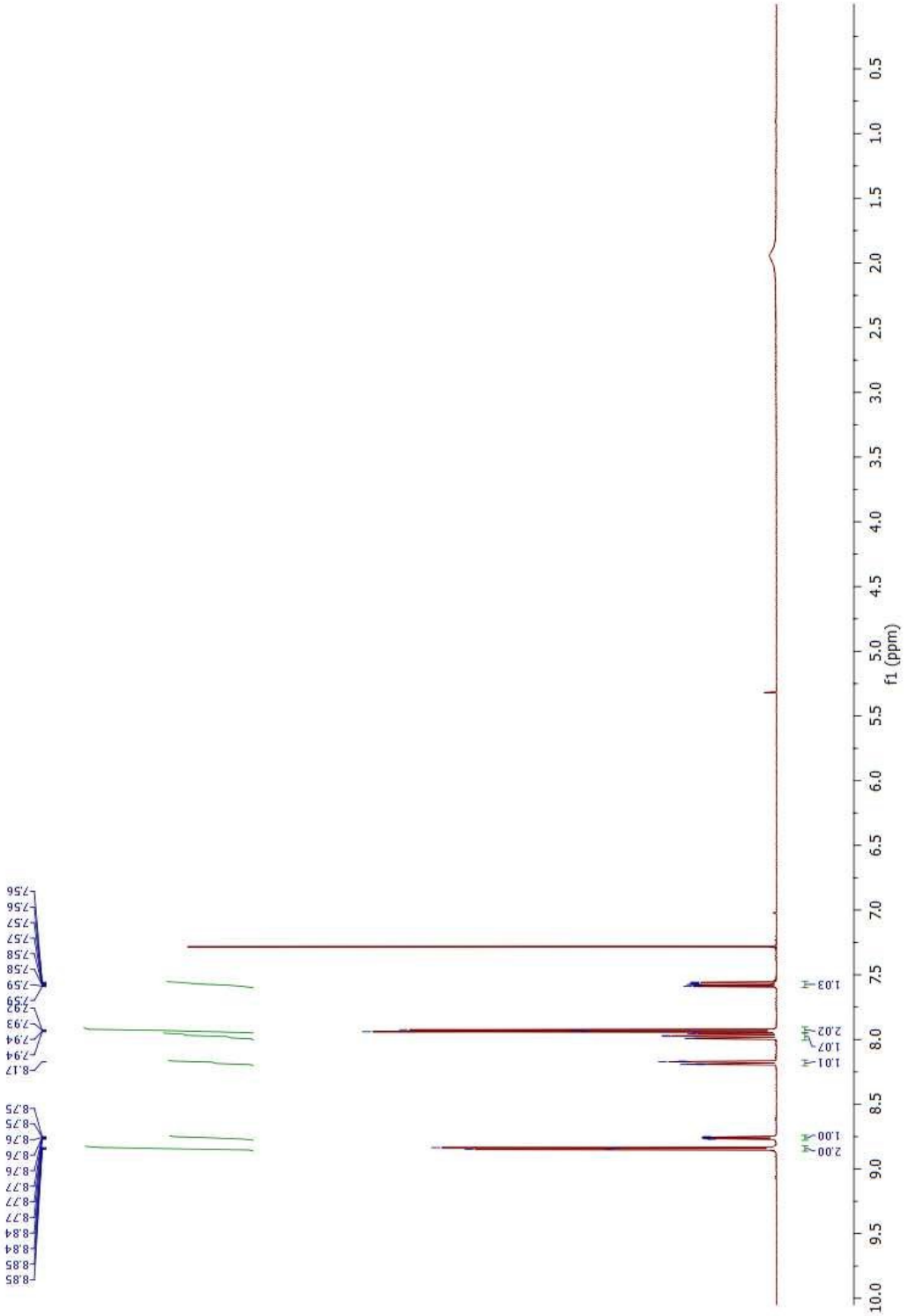

3 ^{13}C NMR in $CDCl_3$

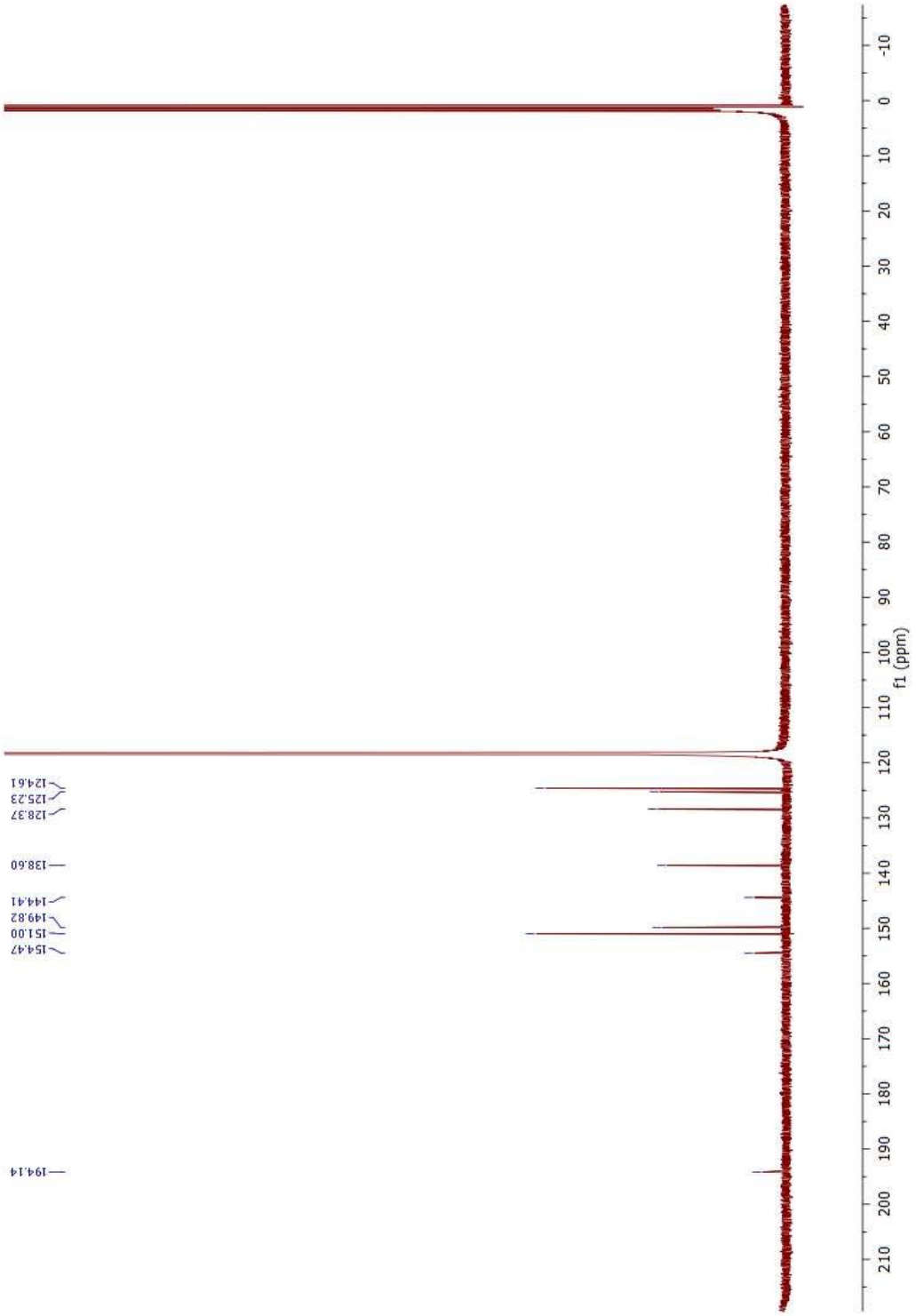

5 ^{1}H NMR in CD_3CN with acetone impurity

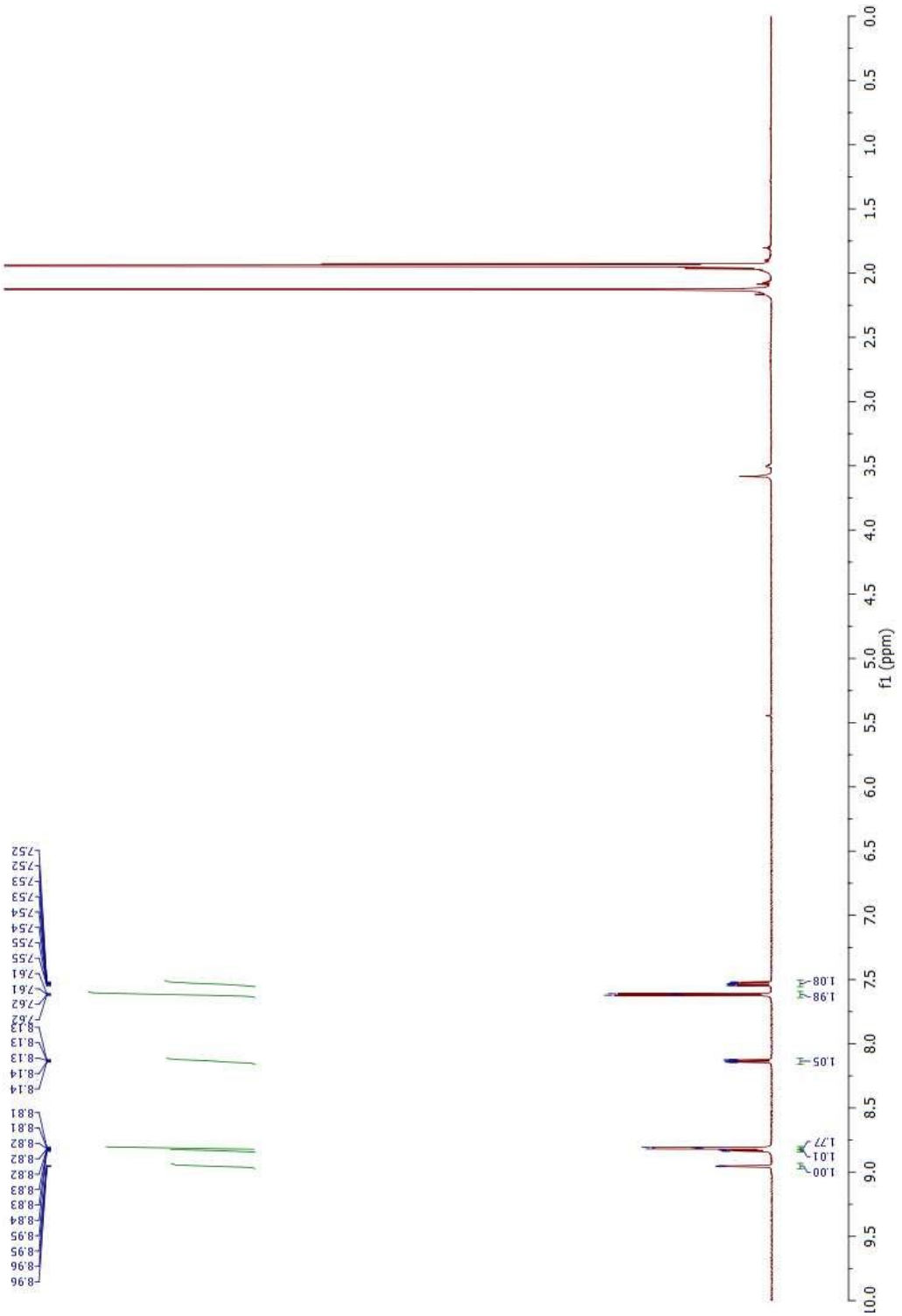

5 ^{13}C NMR in CD_3CN

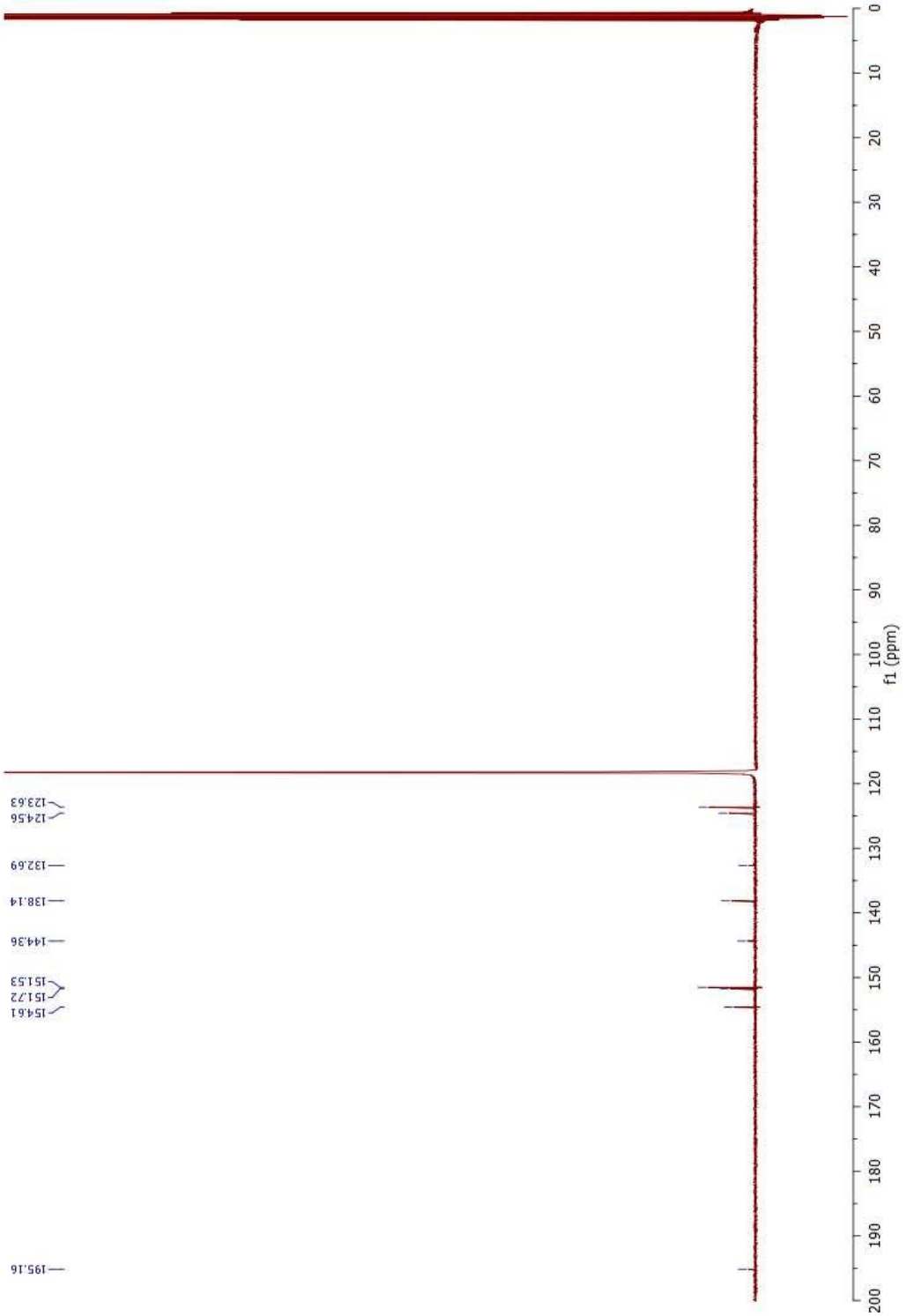

$\mathbf{5}^{2+}$ ^{1}H NMR in CD_3CN

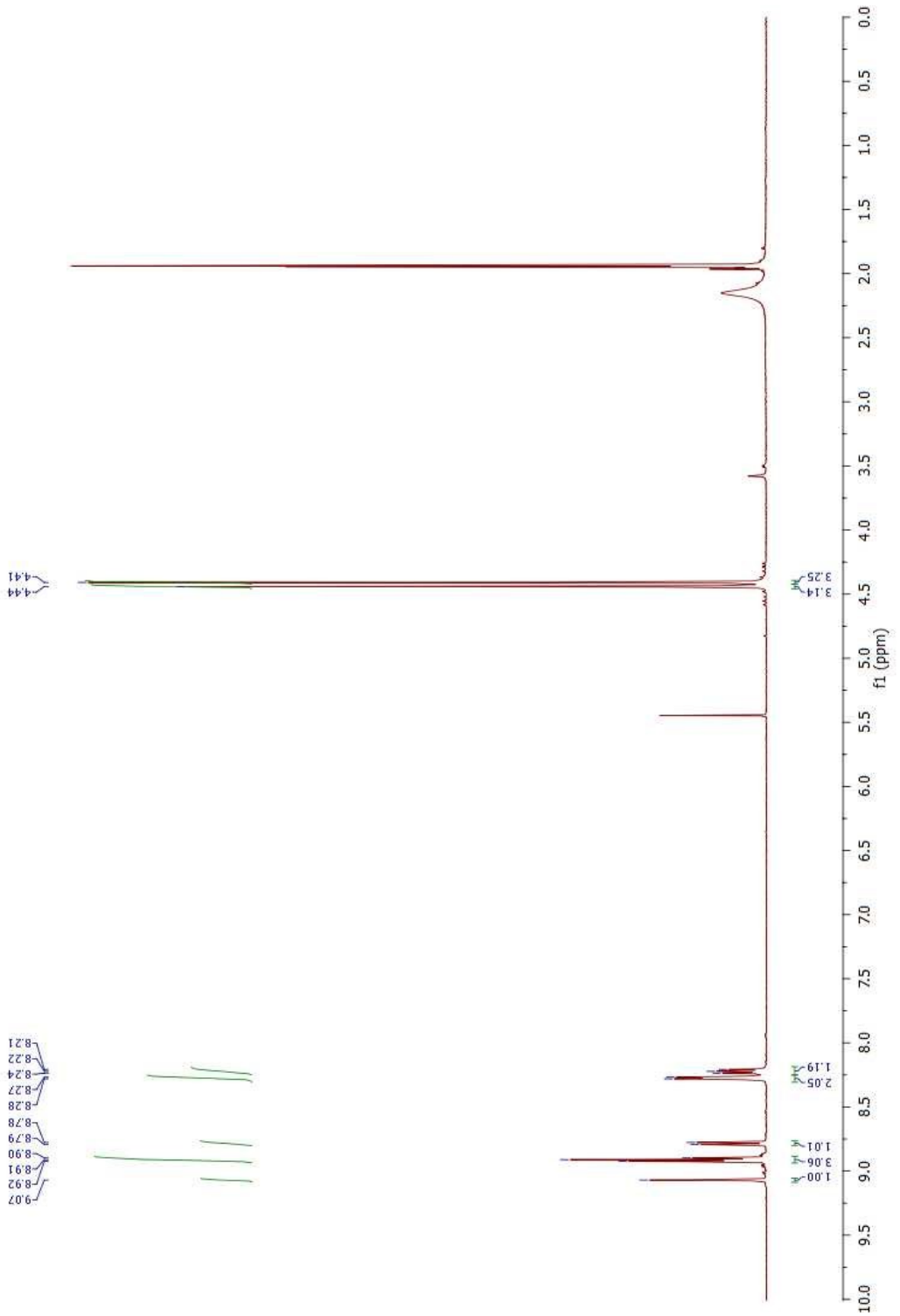

5^{2+} ^{19}F NMR in CD_3CN

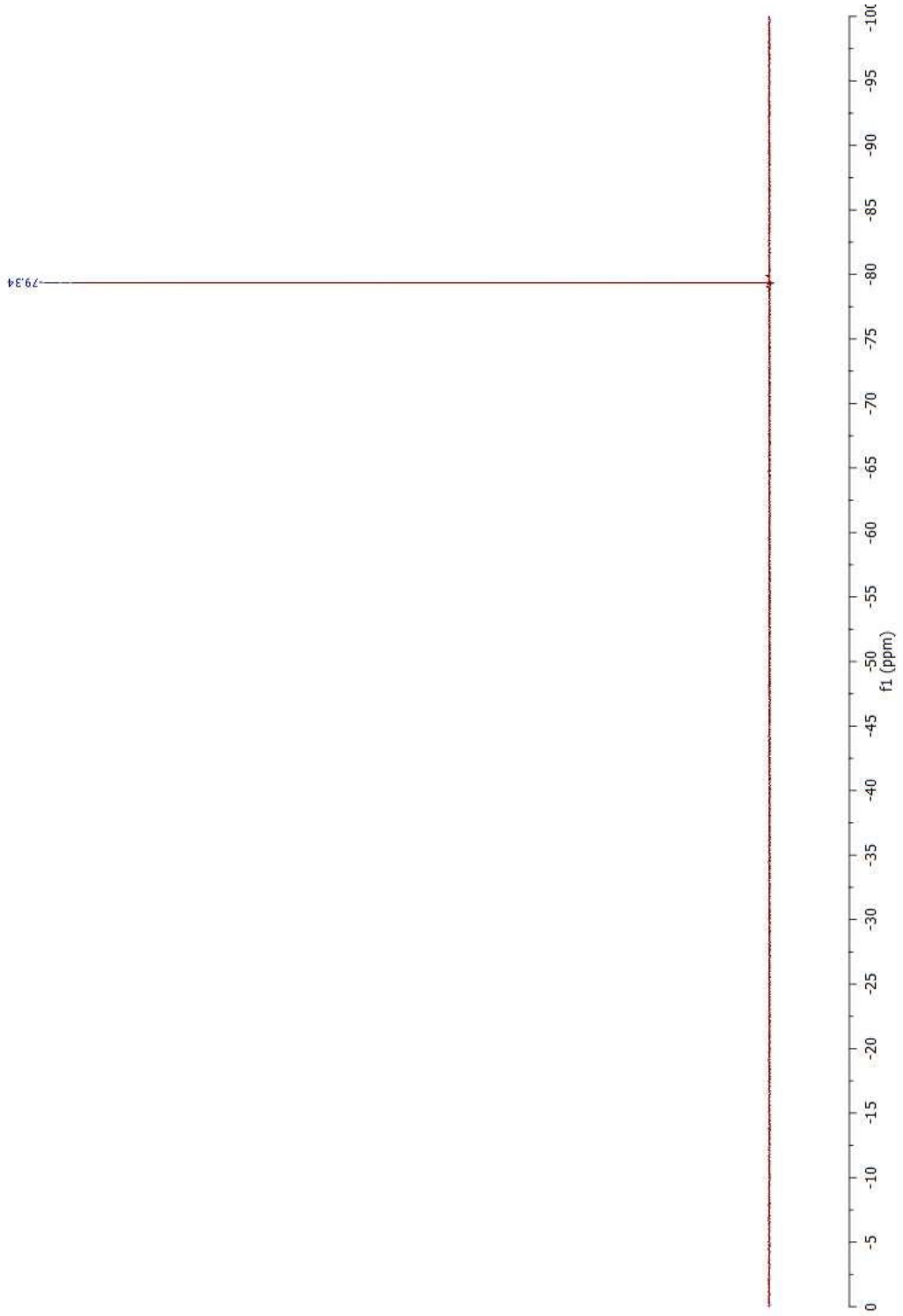

6 ^{1}H NMR in $CDCl_3$

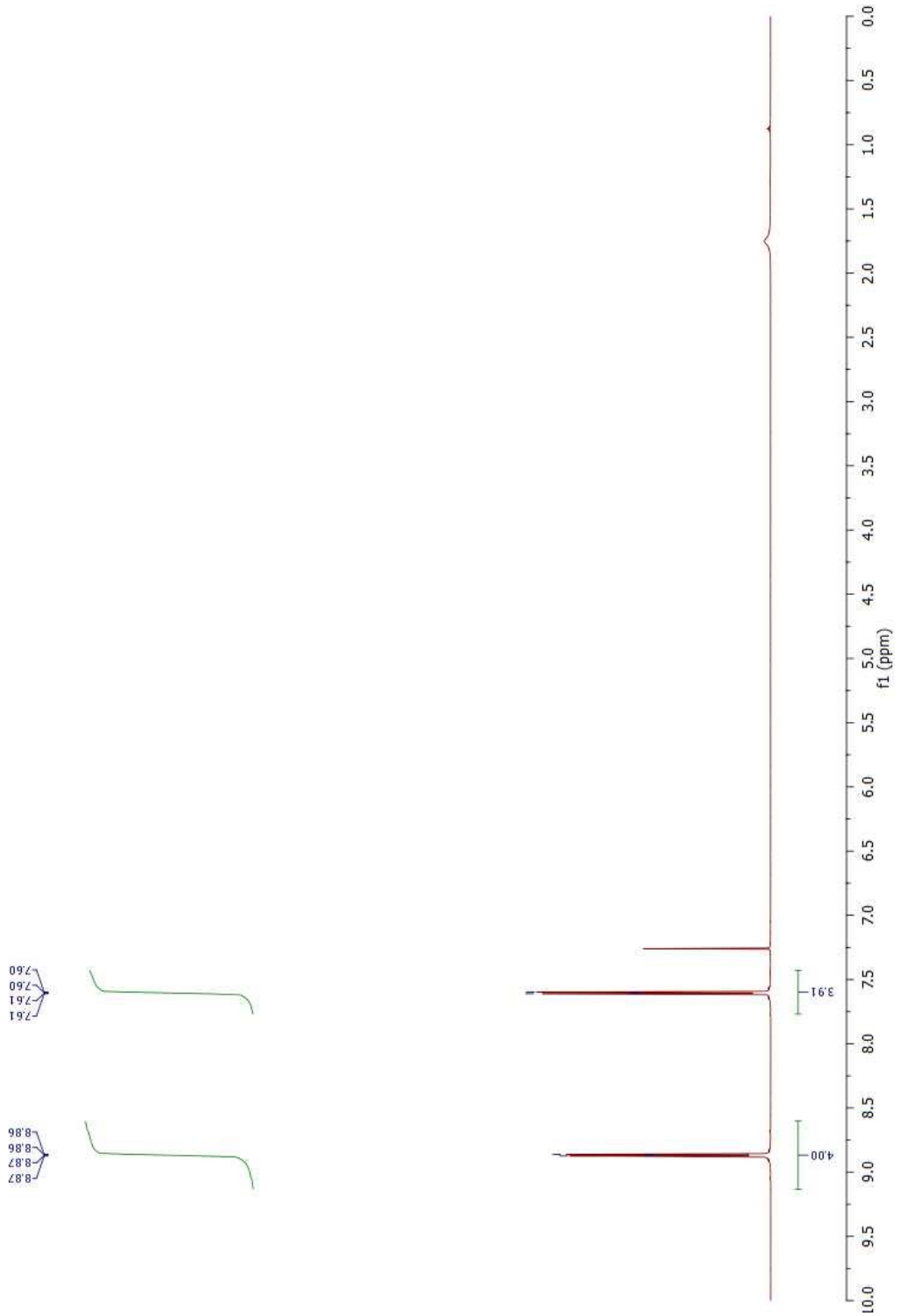

6 ^{13}C NMR in $CDCl_3$

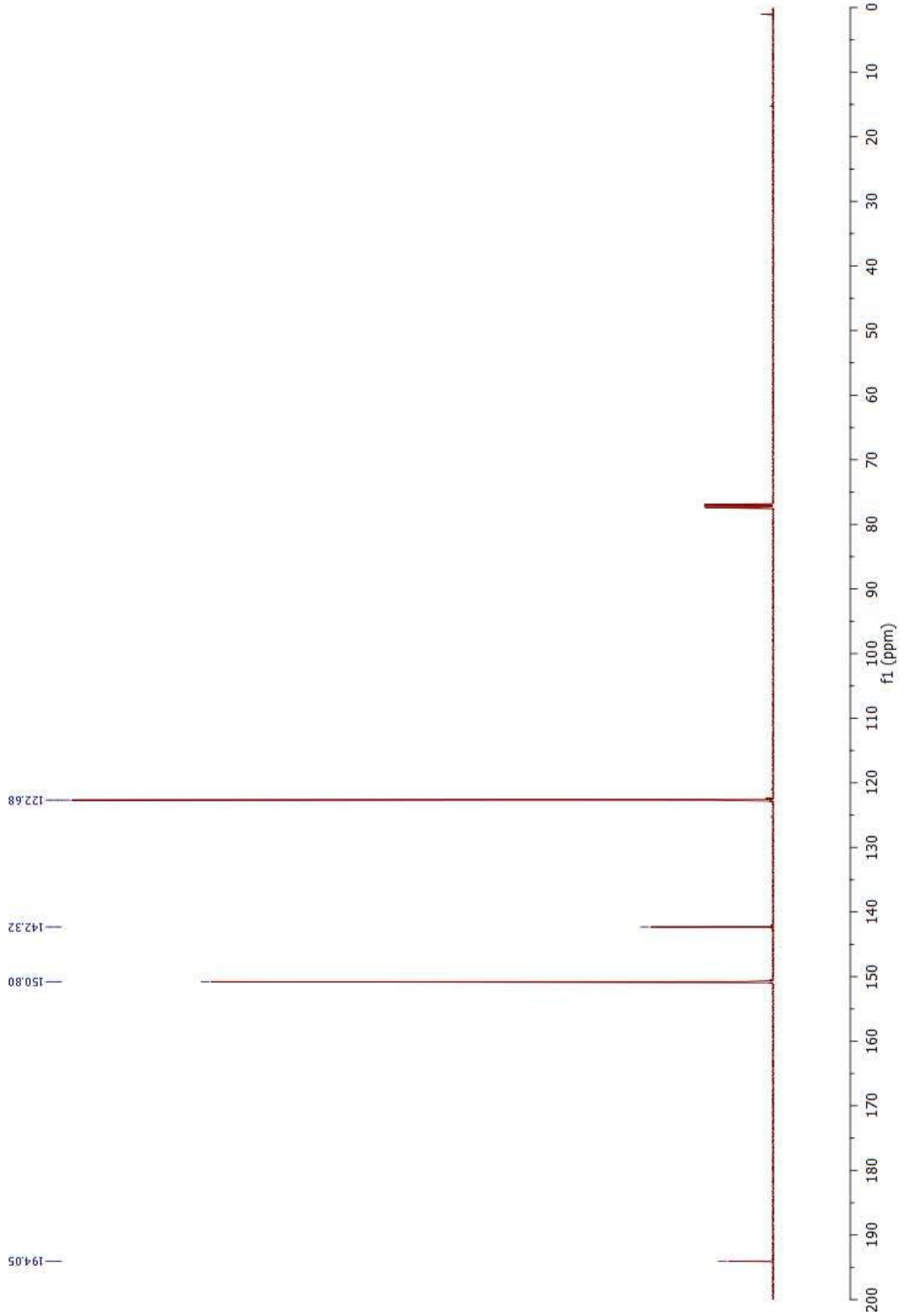

6^{2+} ^{1}H NMR in CD_3CN with DCM impurity

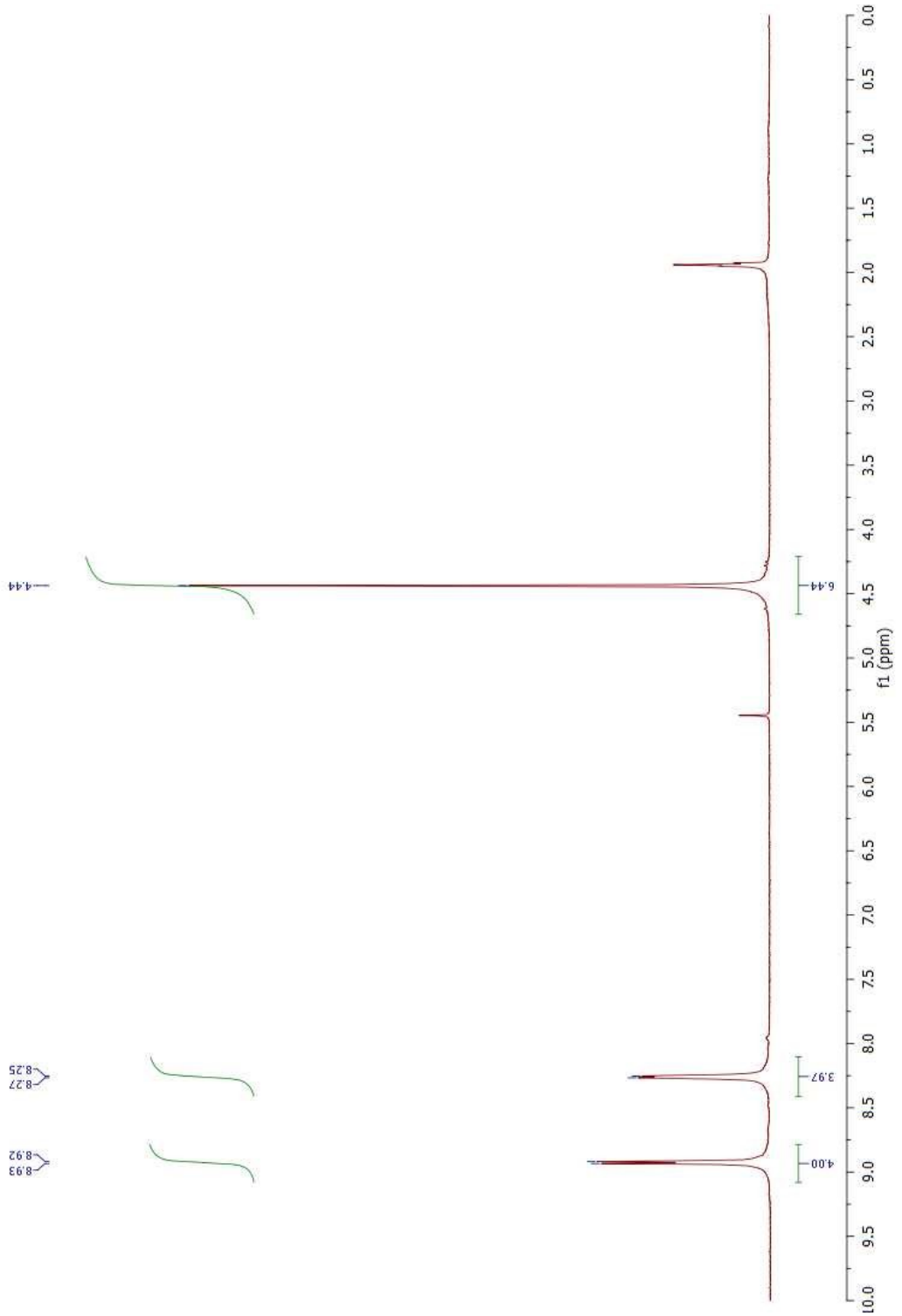

6^{2+} ^{13}C NMR in CD_3CN

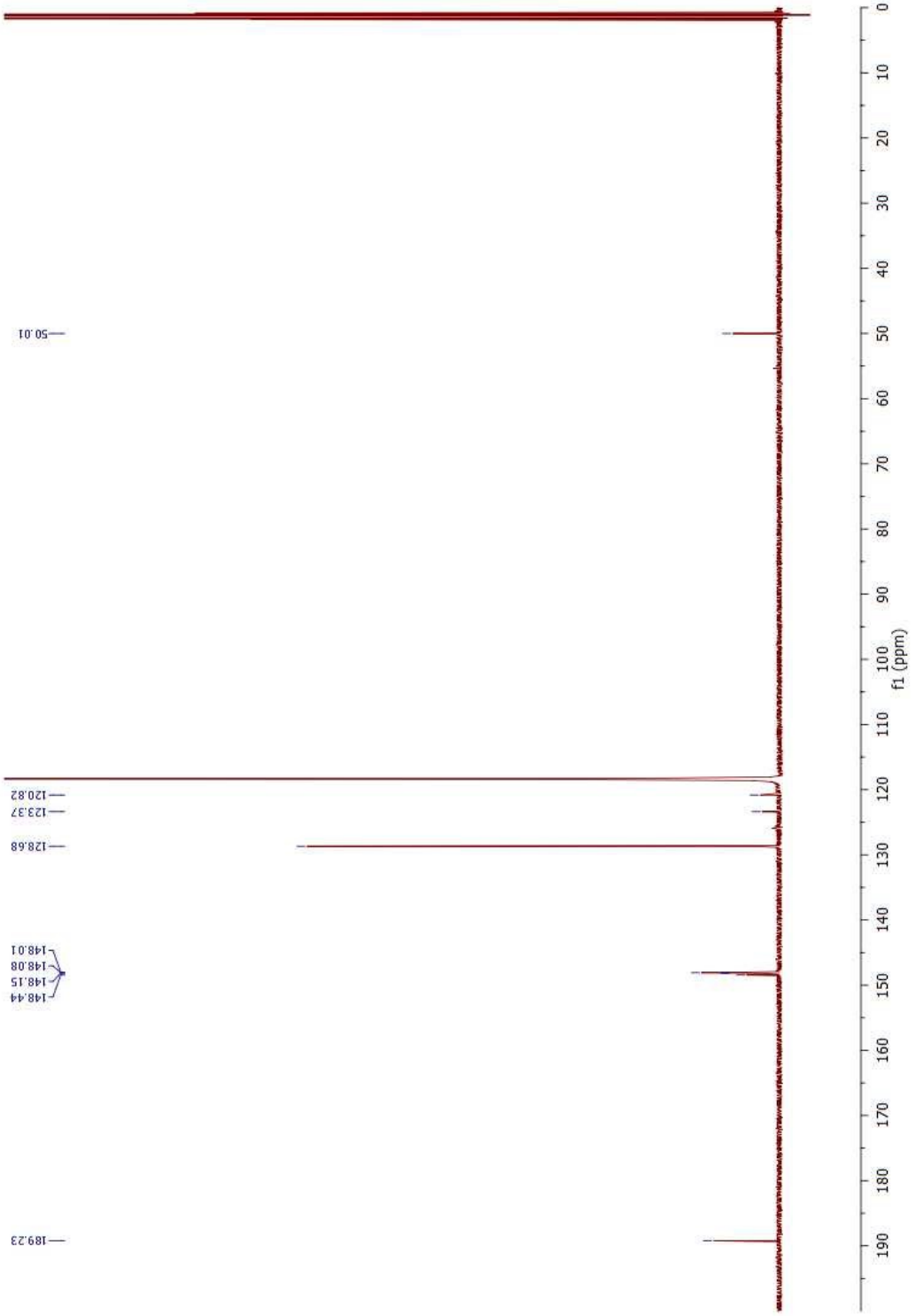

6^{2+} ^{19}F NMR in CD_3CN

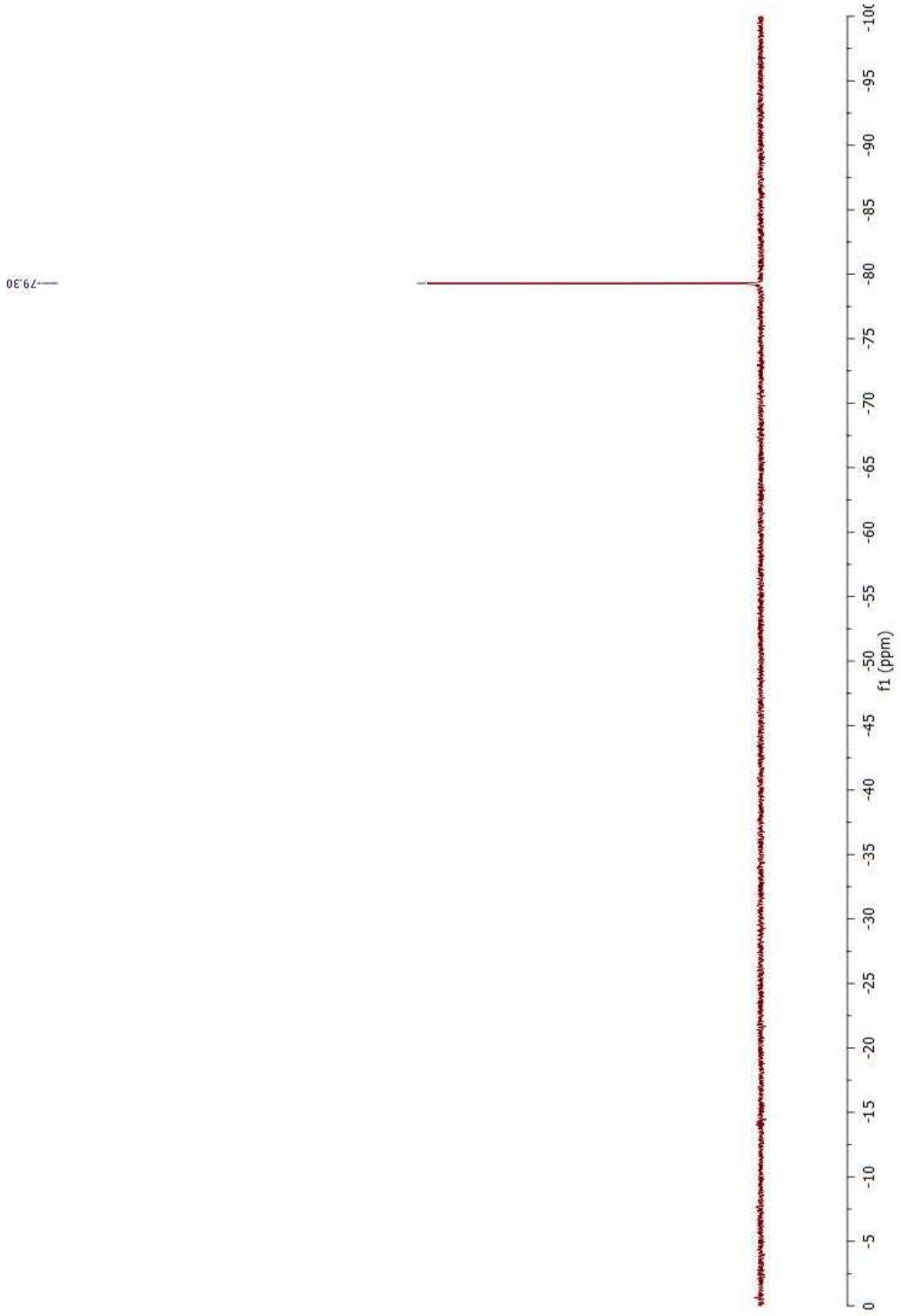

LITERATURE CITED

(1) Ghosh, A. *Letters to a Young Chemist*; 2011.

(2) Alotto, P.; Guarnieri, M.; Moro, F. *Renew. Sustain. Energy Rev.* **2014**, *29*, 325.

(3) Weber, A. Z.; Mench, M. M.; Meyers, J. P.; Ross, P. N.; Gostick, J. T.; Liu, Q. *J. Appl. Electrochem.* **2011**, *41* (10), 1137.

(4) Sada, T.; Sada, T. *Soda to Enso* **2003**, *54* (7,8), 156.

(5) Navalpotro, P.; Palma, J.; Anderson, M.; Marcilla, R. *Angew. Chemie Int. Ed.* **2017**, *56* (41), 12460.

(6) File:Redox Flow Battery.jpg - Wikimedia Commons https://commons.wikimedia.org/wiki/File:Redox_Flow_Battery.jpg (accessed Jun 5, 2018).

(7) Thaller; H., L. Electrically rechargeable REDOX flow cell. 3,996,064, December 7, 1976.

(8) Remick, R. J.; Ang, P. G. P. Electrically rechargeable anionically active reduction-oxidation electrical storage-supply system, November 27, 1984.

(9) Roe, S.; Menictas, C.; Skyllas-Kazacos, M. *J. Electrochem. Soc.* **2016**, *163* (1), 5023.

(10) Skyllas-Kazacos, M.; Rychcik, M.; Robins, R. G.; Fane, A. G.; Green, M. A. *J. Electrochem. Soc.* **1986**, *133* (5), 1057.

(11) Skyllas-Kazacos, M.; Grossmith, F. *J. Electrochem. Soc.* **1987**, *134* (12), 2950.

(12) Kim, K. J.; Lee, H. S.; Kim, J.; Park, M.-S.; Kim, J. H.; Kim, Y.-J.; Skyllas-Kazacos, M. *ChemSusChem* **2016**, *9* (11), 1329.

(13) Li, Y.; Zhang, X.; Bao, J.; Skyllas-Kazacos, M. *J. Energy Storage* **2017**, *11*, 191.

(14) Yan, Y.; Li, Y.; Skyllas-Kazacos, M.; Bao, J. *J. Power Sources* **2016**, *322*, 116.

(15) Yang, Z.; Zhang, J.; Kintner-Meyer, M. C. W.; Lu, X.; Choi, D.; Lemmon, J. P.; Liu, J. *Chem. Rev.* **2011**, *111* (5), 3577.

(16) Project: brine4power https://www.ewe-gasspeicher.de/en/home/b4p (accessed Mar 7, 2018).

(17) Gong, K.; Fang, Q.; Gu, S.; Fong, S.; Li, Y.; Yan, Y. *Energy Environ. Sci. Energy Environ. Sci* **2015**, *8*, 3515.

(18) Egan, S.; Gagstetter, N. *Rio Tinto* **2006**.

(19) Khorsandi, F. *J. Plant Nutr.* **1994**, *17* (9), 1611.

(20) Brown, K. *Water. Air. Soil Pollut.* **1987**, *32* (1–2), 201.

(21) Liu, Q.; Sleightholme, A. E. S.; Shinkle, A. A.; Li, Y.; Thompson, L. T. *Electrochem. commun.* **2009**, *11* (12), 2312.

(22) Sleightholme, A. E. S.; Shinkle, A. A.; Liu, Q.; Li, Y.; Monroe, C. W.; Thompson, L. T. *J. Power Sources* **2011**, *196* (13), 5742.

(23) Sevov, C. S.; Brooner, R. E. M.; Cheard, E.; Assary, R. S.; Moore, J. S.; Rodríguez-Loez, J.; Sanford, M. S. *J. Am. Chem. Soc.* **2015**, *137*, 14465.

(24) Montoto, E. C.; Nagarjuna, G.; Moore, J. S.; Rodriguez-Lopez, J. *J. Electrochem. Soc.* **2017**, *164* (7), A1688.

(25) Wei, X.; Xu, W.; Huang, J.; Zhang, L.; Walter, E.; Lawrence , C.; Vijayakumar, M.; Henderson, W. A.; Liu, T.; Cosimbescu, L.; Li, B.; Sprenkle, V.; Wang, W. *Angew. Chemie* **2015**, *127* (30), 8808.

(26) Duan, W.; Huang, J.; Kowalski, J. A.; Shkrob, I. A.; Vijayakumar, M.; Walter, E.; Pan, B.; Yang, Z.; Milshtein, J. D.; Li, B.; Liao, C.; Zhang, Z.; Wang, W.; Liu, J.; Moore, J. S.; Brushett, F. R.; Zhang, L.; Wei, X. *ACS Energy Lett.* **2017**, *2* (5), 1156.

(27) Shin, S.-H.; Yun, S.-H.; Moon, S.-H. *RSC Adv.* **2013**, *3* (24), 9095.

(28) Hagemann, T.; Winsberg, J.; Grube, M.; Nischang, I.; Janoschka, T.; Martin, N.; Hager, M. D.; Schubert, U. S. *J. Power Sources* **2018**, *378*, 546.

(29) Striepe, L.; Baumgartner, T. *Chem. - A Eur. J.* **2017**, *23* (67), 16924.

(30) Gomberg, M. *J. Am. Chem. Soc.* **1900**, *22* (11), 757.

(31) Michaelis, L.; Hill, E. S. *J. Gen. Physiol.* **1933**, *16* (6), 859.

(32) Elofson, R. M.; Edsberg, R. L. *Can. J. Chem* **1957**, *35*, 646.

(33) Luo, J.; Hu, B.; Debruler, C.; Liu, T. L. *Angew. Chemie, Int. Ed.* **2018**, *57* (1), 231.

(34) DeBruler, C.; Hu, B.; Moss, J.; Luo, J.; Liu, T. L. *ACS Energy Lett.* **2018**, *3* (3), 663.

(35) Murray, C. A.; Zhu, Z.; Cardin, C. J.; Colquhoun, H. M.; Greenland, B. W. *Supramol. Chem.* **2017**.

(36) Gu, Y.; Hong, W.; Choi, W.; Park, J.-Y.; Kim, K. B.; Lee, N.; Seo, Y. *J. Electrochem. Soc.* **2014**, *161* (12), H716.

(37) Burgess, M.; Cheard, E.; Hernadez-Burgos, K.; Nagarjuna, G.; Assary, R. S.; Hui, J.; Moore, J. S.; Rodríguez-Lopez, J. *Chem. Mater.* **2016**, *28*, 7362.

(38) Yang, Y.; Liu, D.; Song, M.; Shi, D.; Liu, B.; Cheng, K.; Lu, Y.; Liu, H.; Yang, M.; Wang, W.; Li, J.; Wei, J. *Chem. - A Eur. J.* **2017**, *23* (31), 7409.

(39) Janoschka, T.; Friebe, C.; Hager, M. D.; Martin, N.; Schubert, U. S. *ChemistryOpen* **2017**, *6* (2), 216.

(40) Burgess, M.; Moore, J. S.; Rodriguez-Lopez, J. *Acc. Chem. Res.* **2016**, *49* (11), 2649.

(41) Hu, B.; Seefeldt, C.; DeBruler, C.; Liu, T. L. *J. Mater. Chem. A Mater. Energy Sustain.* **2017**, *5* (42), 22137.

(42) DeBruler, C.; Hu, B.; Moss, J.; Liu, X.; Luo, J.; Sun, Y.; Liu, T. L. *Chem* **2017**, *3* (6), 961.

(43) Sevov, C. S.; Hickey, D. P.; Cook, M. E.; Robinson, S. G.; Barnett, S.; Minteer, S. D.; Sigman, M. S.; Sanford, M. S. *J. Am. Chem. Soc.* **2017**, *139* (8), 2924.

(44) Doris, S. E.; Ward, A. L.; Baskin, A.; Frischmann, P. D.; Gavvalapalli, N.; Chénard, E.; Sevov, C. S.; Prendergast, D.; Moore, J. S.; Helms, B. A. *Angew. Chemie Int. Ed.* **2017**, *56* (6), 1595.

(45) Hendriks, K. H.; Sevov, C. S.; Cook, M. E.; Sanford, M. S. *ACS Energy Lett.* **2017**, *2* (10), 2430.

(46) Sevov, C. S.; Hendriks, K. H.; Sanford, M. S. *J. Phys. Chem. C* **2017**, *121* (44), 24376.

(47) Baceiredo, A.; Bertrand, G.; Sicard, G. *J. Am. Chem. Soc.* **1985**, *107* (16), 4781.

(48) Arduengo, A. J.; Harlow, R. L.; Kline, M. *J. Am. Chem. Soc.* **1991**, *113* (1), 361.

(49) Braun, M.; Frank, W.; Reiss, G. J.; Ganter, C. *Organometallics* **2010**, *29* (20), 4418.

(50) Makhloufi, A.; Frank, W.; Ganter, C. *Organometallics* **2012**, *31* (20), 7272.

(51) Liske, A.; Verlinden, K.; Buhl, H.; Schaper, K.; Ganter, C. *Organometallics* **2013**, *32* (19), 5269.

(52) Vummaleti, S. V. C.; Nelson, D. J.; Poater, A.; Gómez-Suárez, A.; Cordes, D. B.; Slawin, A. M. Z.; Nolan, S. P.; Cavallo, L. *Chem. Sci.* **2015**, *6* (3), 1895.

(53) Martin, D.; Canac, Y.; Lavallo, V.; Bertrand, G. *J. Am. Chem. Soc.* **2014**, *136* (13), 5023.

(54) Back, O.; Henry-Ellinger, M.; Martin, C. D.; Martin, D.; Bertrand, G. *Angew. Chemie Int. Ed.* **2013**, *52* (10), 2939.

(55) Martin, C. D.; Weinstein, C. M.; Moore, C. E.; Rheingold, A. L.; Bertrand, G. *Chem. Commun.* **2013**, *49* (40), 4486.

(56) Rodrigues, R. R.; Dorsey, C. L.; Arceneaux, C. A.; Hudnall, T. W. *Chem. Commun.* **2014**, *50* (2), 162.

(57) Hudnall, T. W.; Bielawski, C. W. *J. Am. Chem. Soc.* **2009**, *131* (44), 16039.

(58) Blake, G. A.; Moerdyk, J. P.; Bielawski, C. W. *Organometallics* **2012**, *31* (8), 3373.

(59) Deardorff, C. L.; Eric Sikma, R.; Rhodes, C. P.; Hudnall, T. W. *Chem. Commun.* **2016**, *52* (58), 9024.

(60) Mahoney, J. K.; Martin, D.; Thomas, F.; Moore, C. E.; Rheingold, A. L.; Bertrand, G. *J. Am. Chem. Soc.* **2015**, *137* (23), 7519.

(61) Linsker, F.; Evans, R. L. *J. Am. Chem. Soc.* **1946**, *68* (5), 907.

(62) Wibaut, J. P.; Heeringa, L. G. *Recl. des Trav. Chim. des Pays-Bas* **2010**, *74* (8), 1003.

(63) Henze, H. R.; Knowles, M. B. *J. Org. Chem.* **1954**, *19* (7), 1127.

(64) Black, A. L.; Summers, L. A. *J. Chem. Soc. C Org.* **1970**, No. 17, 2394.

(65) Chen, X.-D.; Mak, T. C. W. *Dalt. Trans.* **2005**, No. 22, 3646.

(66) Argyle, V. J.; Woods, L. M.; Roxburgh, M.; Hanton, L. R. *CrystEngComm* **2013**, *15* (1), 120.

(67) Romani, A.; Elisei, F.; Masetti, F.; Favaro, G. *J. Chem. Soc. Faraday Trans.* **1992**, *88* (15), 2147.

(68) Favaro, G.; Romani, A.; Poggi, G. *Zeitschrift für Phys. Chemie* **1990**, *168* (1), 55.

(69) Filipescu, N.; Minn, F. L. *J. Chem. Soc. B* **1969**, 84.

(70) Minn, F. L.; Trichilo, C. L.; Hurt, C. R.; Filipescu, N. *J. Am. Chem. Soc.* **1970**, *92* (12), 3600.

(71) Filipescu, N.; Geiger, F.; Trichilo, C.; Minn, F.; Filipescu, N.; Geiger, F. E.; Trichilo, C. L.; Minn, F. L. *Arch. Biochem. Biophys. Biochem. Pharmacol. J. Chem. Phys* **1967**, *120* (39), 379.

(72) Araujo, R. B.; Banerjee, A.; Panigrahi, P.; Yang, L.; Strømme, M.; Odin, M. S.; Araujo, C. M.; Ahuja, R. *J. Mater. Chem. A Mater. Energy Sustain.* **2017**, *5*, 4430.

(73) Leventis, N.; Rawaswdeh, A.-M. M.; Zhang, G.; Elder, I. A.; Sotiriou-Leventis, C. *J. Org. Chem.* **2002**, *67* (21), 7501.

(74) Johnson III, R. D. *NIST Stand. Ref. Database Number 101* **2015**.

(75) Cramer, C. J. *Essentials of Computational Chemistry Theories and Models*; 2004.

(76) Leventis, N.; Yang, J.; Fabrizio, E. F.; Rawashdeh, A.-M. M.; Oh, W. S.; Sotiriou-Leventis, C. *J. Am. Chem. Soc.* **2004**, *126* (13), 4094.